Modeling a coastal ecosystem to estimate climate change mitigation and a model demonstration in Tokyo Bay

Modeling a coastal ecosystem to estimate climate change mitigation and a model demonstration in Tokyo Bay

Akio Sohma, Hisashi Shibuki, Fumiyuki Nakajima,

Atsushi Kubo, Tomohiro Kuwae

Ecological Modelling 384 (2018) 261–289

Contents lists available at ScienceDirect

Ecological Modelling

journal homepage: www.elsevier.com/locate/ecolmodel

Modeling a coastal ecosystem to estimate climate change mitigation and a model demonstration in Tokyo Bay

Akio Sohma[a,*], Hisashi Shibuki[b], Fumiyuki Nakajima[c], Atsushi Kubo[d], Tomohiro Kuwae[e]

[a] Graduate School of Engineering, Osaka City University, 3-3-138 Sugimoto, Sumiyoshi-ku, Osaka, 558-8585, Japan
[b] Science Solutions Division, Mizuho Information & Research Institute, Inc., 2-3 Kanda-Nishikicho, Chiyoda-ku, Tokyo, 101-8443, Japan
[c] Graduate School of Engineering, The University of Tokyo, 7-3-1 Hongo, Bunkyo-ku, Tokyo, 113-8656, Japan
[d] Department of Geosciences, Shizuoka University, 836 Ohya, Suruga-ku, Shizuoka 422-8529, Japan
[e] Coastal and Estuarine Environment Research Group, Port and Airport Research Institute, 3-1-1 Nagase, Yokosuka, 239-0826, Japan

ARTICLE INFO

Keywords:
CO_2 uptake
Carbon burial
Carbonate chemistry
Carbon-nutrient-oxygen cycles
Food web
Benthic-pelagic coupling

ABSTRACT

An ecosystem model called the "EMAGIN-B.C. ver 1.0 (Ecosystem Model for Aquatic Geologic Integrated Network for Blue Carbon)", describing the Carbon-Nitrogen-Phosphorus-Oxygen-Calcium cycle was developed to estimate/predict carbon capture and storage in estuaries. EMAGIN-B.C. analyzes (1) carbon burial, wherein carbon is captured biologically in the pelagic and benthic ecosystems and stored in deeper sediments, (2) CO_2 uptake at the ocean surface while considering the carbonate chemistry with total alkalinity and Dissolved Inorganic Carbon (DIC) production/consumption due to biochemical processes, (3) DIC capture associated with grazing at the trophic level among phytoplankton, zooplankton, and benthic fauna, (4) the effects of hypoxia on benthic fauna and bacteria by precise modeling of the biochemical oxygen production/consumption and the resultant hypoxia, and (5) the carbon transport by integration with the hydrodynamic model. EMAGIN-B.C. was applied to Tokyo Bay, a eutrophic, shallow coastal area, and reproduced the observations well. From the model outputs, it can be observed that Tokyo Bay shows functions of climate change mitigation. In the one-year carbon budget, Tokyo Bay captured 16.6% of the DIC from the atmosphere and river as organic matter by biological processes, and 3.9% of the total carbon flowing from the atmosphere and river was stored in the deeper sediment layer.

1. Introduction

Fossil fuel combustion and changes in land use after the industrial revolution have been known to destabilize the carbon equilibrium state between the atmosphere and ocean on a global scale, and it is estimated that it will take several millennia to regain equilibrium (Hoffert et al., 1979). The global ocean contains approximately 50 times more carbon than does the atmosphere (Archer and Brovkin, 2008), and it is an important sink of atmospheric CO_2 (Houghton and Intergovernmental Panel on Climate Change. Houghton, 2001). Major global carbon reservoirs are comprised of the atmosphere, oceans, terrestrial biosphere, fossil fuels, and lithosphere (kerogens and sedimentary rocks), among which the oceans are the second largest reservoir (Falkowski et al., 2000; Solomon, 2007; McLeod et al., 2011). However, it is unclear whether the carbon reserved/sequestered by the shallow coastal waters comprised of estuaries, shallows, salt marshes, seagrass, mangroves, and intertidal flats have been included in these past estimations (McLeod et al., 2011). Recently, despite their relatively small areal coverage of 0.5% of the global earth (UNEP), several studies have focused on exploring the potential of shallow coastal waters as carbon reservoirs (stocks) and sinks (flows) due to their dense biological activities. (Alongi et al., 2016; Chen et al., 2013; Chmura et al., 2003; Donato et al., 2011; Fourqurean et al., 2012; Frankignoulle et al., 1998; Kubo et al., 2017; Kuwae et al., 2016; Murdiyarso et al., 2015)

Our definition of ocean functions for carbon capture and storage, the so-called "climate mitigation functions of the ocean" are those classified into (1) a CO_2 uptake function, (2) a Dissolved Inorganic Carbon (DIC) capture function, and (3) a carbon storage function (Fig. 1). The CO_2 uptake function is absorption of atmospheric CO_2 into the ocean by an air-sea CO_2 gas exchange (physical CO_2 uptake), while the DIC capture function is temporally fixing DIC as organisms or as $CaCO_3$ by biological production (biological DIC capture), and the carbon storage function is long-term (on a geological time scale) carbon sequestration deep into the sediment. When considering the shallow coastal water as composed of benthic and pelagic systems and focused on captured and stored carbon stocks within the ecosystem, the amount of carbon remaining in the system results in the following fluxes: Flux 1 is the burial of the particulate organic carbon (POC, comprised of detritus) and calcium carbonate ($CaCO_3$) into a sedimentation zone on a geological time scale; Flux 2 is the air-sea CO_2 gas exchange; Flux 3 is inflows of POC, dissolved organic carbon (DOC), and DIC (which is

* Corresponding author at: #C321, Graduate School of Engineering, Osaka City University, 3-3-138, Sugimoto, Sumiyoshi-ku, Osaka, 558-8585, Japan.
E-mail address: sohma@eng.osaka-cu.ac.jp (A. Sohma).

https://doi.org/10.1016/j.ecolmodel.2018.04.019
Received 7 January 2018; Received in revised form 28 April 2018; Accepted 28 April 2018
Available online 17 July 2018

comprised of $CO_{2,aq}$, H_2CO_3, HCO_3^-, and CO_3^{2-}) from the river; and Flux 4 is the inflow/outflow of POC, DOC, $CaCO_3$, and DIC into the continental shelf or deep sea (Fig. 1). Here, the effects of the input of DIC and DOC through groundwater flow and volcanic activity, the subtraction of DIC, and the DOC associated with non-resident fish are omitted in Fig. 1 and are also currently excluded from our research objectives. If the value of Flux 1, burial, is higher, the geological time scale carbon stock that exists as fossil fuels and $CaCO_3$ in the shallow coastal system increases. If the sum of Fluxes 2, 3, and 4 is positive, the temporal carbon stock in the shallow coastal area increases, and, conversely, it decreases if the sum of the fluxes is negative. The flux directly affecting atmospheric CO_2 is Flux 2, and its effect is relatively in the short-term. In contrast, Flux 1 affects atmospheric CO_2 indirectly but long-term. Fluxes 3 and 4 affect Fluxes 1 and 2 through the biochemical and physical processes in the shallow coastal ecosystem.

As for the value of Flux 1, burial rates of organic carbon in vegetated shallow coastal waters are exceptionally high, exceeding those in the soils of terrestrial forests by 30- to 50-fold (Duarte et al., 2013). Globally, coastal vegetated habitats and terrestrial forests bury comparable amounts of organic carbon annually, despite the extent of coastal marine vegetation being less than 3% of forests, although this estimated value has great uncertainty (Duarte, 2017; Duarte and Cebrian, 1996; Duarte et al., 2005). As for the value of Flux 2, some shallow coastal waters are recognized to be net emitters of CO_2 to the atmosphere through air-sea CO_2 gas exchange (Borges and Abril, 2011; Cai, 2011; Chen et al., 2013; Laruelle et al., 2013); however, some studies have indicated CO_2 uptake (Kone et al., 2009; Kubo et al., 2017; Kuwae et al., 2016). In terms of Flux 3, Chen et al. (2012) estimated the air-sea CO_2 gas exchange from the head to the mouth of large river estuaries and concluded that the head of the estuary is a strong CO_2 source while the mouth of the estuary functions as a large CO_2 sink. Kuwae et al. (2016) also argued that the nutrient load from rivers affects the air-sea CO_2 gas exchange. In terms of Flux 4, several sources estimate the inflow/outflow of DOC, DIC, and POC in terms of the carbon stock of shallow coastal areas based on observations or budget models (Algesten et al., 2006; Eyre and McKee, 2002; Kubo et al., 2015; Mahmud et al., 2017).

In general, estimations of Fluxes 1, 2, 3, 4, and shallow coastal carbon stock are derived from the limited observations and statistical analyses on each flux. In addition, available observational data from particular systems are insufficient to cover the large spatial and temporal variability of carbon cycles. Furthermore, Fluxes 1, 2, 3, 4, and the carbon stock of shallow coastal areas are influenced by biological DIC capture flux, Flux 5 in Fig. 1, and all these factors are the result of interactions between physical and biochemical processes in the shallow coastal ecosystem. Therefore, the ecosystem model describing the physical and biochemical processes, i.e., the ecological connectivity, is a powerful tool (1) to understand the spatio-temporal patterns and variability, (2) to pursue the key mechanisms and interactions, and (3) to predict the ecosystem response to environmental measures. In addition, the model's representation of the results from the ecological connectivity enables us to reveal the unknown partial processes from the dynamics of the whole ecosystem. In fact, while taking into account the above advantages of the ecosystem model, a number of ecosystem models describing the ocean biogeochemistry and the lower trophic levels of the food web have emerged over the last two decades, in a variety of contexts ranging from simulations of batch cultures or mesocosms over the shallow coastal waters to the global ocean (Aumont et al., 2003; Butenschoen et al., 2016; Fasham et al., 1990; Flynn, 2010; Geider et al., 1997; Stock et al., 2014; Wild-Allen et al., 2010; Yool et al., 2013; Zavatarelli and Pinardi, 2003).

When the ecosystem model is applied to shallow coastal waters with high biological productivity and is used to reveal the spatiotemporal dynamics of Fluxes 1–5 (Fig. 1) as results of ecological connectivity, it is significant for it to satisfy the following requirements simultaneously:

I Coupling the benthic and pelagic ecosystems to demonstrate the series of processes in which carbon is captured in water or sediment surfaces and is stored in deeper sediments.
II Describing the food web of detritus, phytoplankton, zooplankton, and benthic fauna to estimate the carbon capture function associated with grazing at the trophic level.
III Incorporating the carbonic chemistry theory among DIC, total alkalinity, pH, and partial pressure of CO_2 (pCO_2) while describing detailed alkalinity production/consumption through biochemical processes to estimate the air-sea CO_2 gas exchange.
IV Treating Carbon-Nitrogen-Phosphorus-Oxygen-Calcium coupled cycles to estimate the biological production that affects the biological DIC capture functions.
V Describing the vertical profiles of biochemical processes at micro-scales (mm-scale pitch) in the sediments related to oxygen consumption/production to demonstrate the effects of hypoxia on (a) benthic fauna (its mortality processes), which affects the biological DIC capture functions, and (b) bacterial processes such as the oxic, suboxic, and anoxic mineralization and re-oxidation of the Oxygen Demand Unit (ODU, comprised of Mn^{2+}, Fe^{2+}, and S^{2-}; Soetaert et al., 1996), which affect the alkalinity production/consumption.

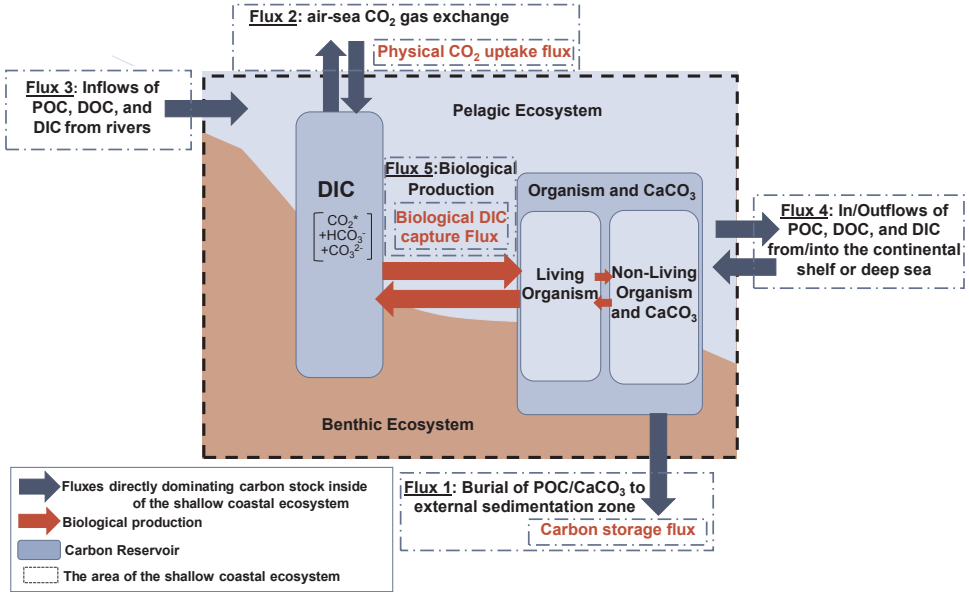

Fig. 1. The five fluxes dominating the dynamics of carbon stock in the shallow coastal area. The area inside the dotted line is the shallow coastal ecosystem, which is the target of estimation.

VI Integration with the hydrodynamic model to estimate the carbon transport in the estuary and at the offshore boundary.

Most of the ecosystem models treating the coupling of the benthic and pelagic ecosystems were produced with an emphasis on studying eutrophication (Cerco et al., 2006; Fennel et al., 2011; Lancelot et al., 2005; Meire et al., 2013; Reed et al., 2011; Soetaert et al., 2001; Soetaert and Middelburg, 2009; Yakushev et al., 2017). The biochemical processes considered in these models are mainly the bacterial biogeochemical processes, due to their focus on deoxygenation and redox biogeochemistry at the sediment and sediment-water interface. Thus, they treat vertical micro-profiles of biochemical processes and do not treat the benthic fauna explicitly. As for the food-web modeling, currently, one of the most well-known and established coupled models is the European Regional Seas Ecosystem (ERSEM) model, which demonstrates C-N-O-P-Si-Fe coupled cycles and the food web, including benthic fauna (Butenschoen et al., 2016). As for the carbonate chemistry, biochemical processes can lead to either an increase or decrease of both DIC and alkalinity (Soetaert et al., 2007; Wolf-Gladrow et al., 2007), and there exist various treatment methods especially for alkalinity production/consumption. For example, the Bottom RedOx Model (BROM) (Yakushev et al., 2017) and the Dream OceaN Global Research Integration model (DONGRI) (Sohma et al., 2005) treat the total alkalinity as a model variable and calculate the increase and decrease of alkalinity due to the oxidization/reduction linked to biogeochemical processes. ERSEM treats the nutrient concentration effect on the alkalinity (Artioli et al., 2012).

The model "EMAGIN-B.C. ver 1.0″ (the Ecosystem Model for Aquatic Geologic Integrated Network for Blue Carbon), introduced herein, is unique in that it simultaneously meets all the requirements in items I to VI. The objectives of EMAGIN-B.C. are to demonstrate the spatiotemporal dynamics of Flux 1, the burial of POC and $CaCO_3$; Flux 2, the air-sea CO_2 gas exchange (physical CO_2 uptake); Flux 3, inflows of POC, DOC, and DIC from rivers; Flux 4, the inflow/outflow of POC, DOC, $CaCO_3$ (carbon storage), and DIC into the continental shelf or deep sea; and, lastly, Flux 5, biological production (biological DIC capture) to estimate/predict the carbon stock of the estuary. The final goal of EMAGIN-B.C. is to reveal the mechanisms/interactions of biochemical-physical processes linked to carbon stock in various shallow coastal areas, such as salt marshes, sea grass beds, tidal flats, mangroves, coral reefs, and urbanized enclosed estuaries and fjords and to estimate/predict their mitigating effects on climate change.

As a first step, EMAGIN-B.C. ver 1.0 was developed and applied to Tokyo Bay, whose coastal type is classified as a eutrophic, semi-closed estuary with river inflows. Tokyo Bay was chosen because the ecosystem is less complex, and comprehensive observed data were present, as compared to in other shallow vegetated coastal areas. In this paper, we introduce the EMAGIN-B.C. ver 1.0 model and validate the model by application to Tokyo Bay. In addition, we demonstrate the carbon stock, CO_2 uptake, DIC capture, and carbon storage functions of Tokyo Bay through an analysis of the carbon cycle mechanisms derived from EMAGIN-B.C.

2. Model description

EMAGIN-B.C. was developed based on the previous developed ecological connectivity hypoxia model (Sohma et al., 2008), referred to here as EMAGIN-E.H. (the Ecosystem Model for Aquatic Geologic Integrated Network for Eutrophication and Hypoxia), which focused on the estimation and prediction of the eutrophication/hypoxia effect on the estuaries with respect to (1) the linkage of the benthic and pelagic ecosystems, (2) the food-web structure among detritus, phytoplankton, zooplankton, and benthic fauna, (3) the description of the C-N-P-O coupled cycles, (4) the description of the benthic vertical micro-scale variations of the benthic biogeochemical processes, such as the oxic, suboxic, and anoxic mineralization, denitrification, nitrification, and oxidation of ODU (Mn^{2+}, Fe^{2+}, S^{2-}), and (5) the interaction between the central bay (hypoxic area) and tidal flat ecosystems. The processes added to EMAGIN-B.C. that did not exist in EMAGIN-E.H. are in the carbonate system, including (1) the carbonate chemistry theory among DIC, total alkalinity (TALK), pCO_2, and pH, (2) DIC and TALK production/consumption due to biochemical processes in the benthic and pelagic systems, and (3) the formation/dissolution of $CaCO_3$. As a result, EMAGIN-B.C. represents mechanistically the dynamics of carbon capture and storage functions in the shallow coastal area as a result of the linkage among the carbon-nutrients-oxygen cycling system, the food-web system, and the carbonate chemistry system.

EMAGIN-B.C. is composed of two models: a hydrodynamic model and an ecological model. The analysis flow of EMAGIN-B.C. and the forcing factors of the hydrodynamic and ecological models are illustrated in Fig. 2. Through coupling with the hydrodynamic model, EMAGIN-B.C. can estimate the carbon transport within the estuary and at the offshore boundary of the estuary.

2.1. Hydrodynamic model

The hydrodynamic model simulates the three-dimensional physical field in the pelagic system of the estuary and demonstrates long-term variability of the flow field, salt, and heat transport. The driving forces of the flow field considered in the model are tidal forces, surface winds, and the local density gradient with realistic coastal topography and bathymetry. An overview of the model is shown in Appendix F. More details on the hydrodynamic model are well described by Nakata et al. (1983a, 1983b) and Sohma et al. (2008). The target area is a mesoscale estuary (1–100 km^2) defined as a semi-enclosed shallow coastal water body where seawater mingles with freshwater from rivers (Pritchard, 1967).

2.2. Ecological model

The ecological model is a system of equations that establishes the components governing the dynamics of the coastal carbon stock and its related environmental phenomena as model variables. The model describes the interaction among model variables as the transformations that C, N, P, Ca, and O_2 undergo as the result of biochemical processes while considering the physical transport. The dynamics and spatial distribution of the model variables are described by partial differential equations (refer to Appendix A). The equations satisfy the mass conservation of C, N, P, Ca, and O_2 and are comprised of the production and consumption terms of biochemical processes and transport terms triggered by physical processes. Each path of the C-N-P-Ca-O coupled cycle (as biochemical processes) is derived from empirical and experimental formulations. The formulations of each biochemical reaction are based on a first order reaction and include (a) several model variables, (b) environmental variables obtained from prescribed functions and data (e.g., temperature, light intensity), (c) biochemical parameters, and (d) universal constants. The values of the biochemical processes are calculated and changed at each time step. Changes in the biochemical processes affect the dynamics and spatial distribution of the model variables and vice versa. The ecological model simulates the ecosystem dynamics as the result of this entanglement of various interactions. The biochemical processes and model variables treated in EMAGIN-B.C. are described in Fig. 3(a) and (b) (refer to Appendix B for details).

2.3. Biochemical processes

We focus on biochemical processes affecting the climate change mitigation function (i.e., physical CO_2 uptake, DIC biological capture, and carbon storage in Fig. 1) conceptually. It includes three systems: (a) the carbon-nutrients-oxygen cycling system comprised of plankton primary production and bacterial biogeochemical processes, (b) the food-web system from planktons to benthic fauna and detritus to benthic fauna, and (c) the carbonate chemistry system among DIC (which is comprised of CO_2^* (i.e., sum of CO_{2aq} and H_2CO_3), HCO_3^-, and CO_3^{2-}), and pH. The three systems are linked to each other and govern the climate change mitigation function.

The conceptual-simplified diagram related to the climate change

mitigation function comprised of the three systems in the shallow coastal areas are shown in Fig. 4. The red arrows indicate DIC increase/decrease mechanisms linked to CO_2 uptake/release and POC burial mainly dominated by the carbon-nutrients-oxygen cycling system and the food-web system. The blue arrows indicate alkalinity increase/decrease mechanisms linked to CO_2 uptake/release and $CaCO_3$ burial mainly driven by the carbonate chemistry system and the food-web system (i.e., shell formation). Both DIC and alkalinity increases/decreases result in changes in pCO_2 and pH (Millero, 1995). pCO_2 at the ocean surface is the governing element of CO_2 uptake/release at the ocean surface, as formulated below:

$$F_s = E(pCO_{2,water} - pCO_{2,air}) \quad (1)$$

where F_s is the CO_2 uptake/release flux at the ocean surface (the net-flux of CO_2 between the air and sea systems) [μgC·cm^{-2}·s^{-1}], E is the gas exchange coefficient [μgC·cm^{-2}·s^{-1} μatm^{-1}], and $pCO_{2,\ water}$ and $pCO_{2,\ air}$ are the partial pressures in the surface-water and in the atmosphere [μatm], respectively. For E, there are several empirical functions, such as the function for wind speed (Wanninkhof and McGillis, 1999) and the function for temperature and salinity (Sorai and Ohsumi, 2005), both of which can be selected in the model (Appendix C). The model's descriptions of the three systems are as follows.

2.3.1. Carbon-nutrients-oxygen cycling system

The photosynthetic and biogeochemical processes connecting phytoplankton–zooplankton–detritus–dissolved organic matter (DOM)–nutrients (NH_4-N, NO_3-N, PO_4-P)–dissolved oxygen are the same as in EMAGIN-E.H. (Sohma et al., 2008). The processes are formulated based on a first-order reaction formula multiplied by functions of (1) the nonlinear or linear reactions that represent the limitations of light intensity in photosynthesis and the limitations or inhibitions of model variables (e.g., nutrient limitation in photosynthesis, oxygen limitation in oxic mineralization and nitrification) and (2) the response to temperature. The formulations are described in Tables B6 and B7 in Appendix B.

2.3.2. Food-web system

The benthic fauna is divided into suspension feeders and deposit feeders. In the model, suspension feeders feed on particulate organic matter (i.e., phytoplankton, zooplankton, detritus, and DOM), while deposit feeders feed on detritus and DOM in the benthic system. The parts of the feeding phytoplankton/zooplankton/detritus/DOM are assimilated as the feeders' biomass. The mortality of benthic fauna due to hypoxia were considered/formulated to estimate the effect of hypoxia on benthic fauna for climate-change mitigation (Table B7 in Appendix B).

2.3.3. Carbonate chemistry system

As for the carbonate chemistry system, inorganic carbonate chemistry and partial pressure physics are well understood and can be reproduced with fair accuracy even in a simple carbonate chemistry theory that considers the chemical relations among DIC (which is comprised of CO_2^*, HCO_3^-, and CO_3^{2-}), TALK, pCO_2, and pH to be at chemical equilibrium (Hoffert et al., 1979; Millero, 1995; Dickson, 1981, 1990; Dickson et al., 2007; Mehrbach et al., 1973). At each time step of calculation, EMAGIN-B.C. first calculates the production/consumption of DIC (i.e., the sum of CO_2^*, HCO_3^-, and CO_3^{2-}) and TALK due to biochemical processes treated in the carbon-nutrients-oxygen cycling system, as well as due to $CaCO_3$ formation/dissolution, by using the stoichiometric relations shown in Table 1. Then, pCO_2 and pH are solved from DIC and TALK through the theory of inorganic carbonate chemistry, using chemical equilibrium constants among CO_2^*, HCO_3^-, and CO_3^{2-}. Here, the chemical equilibrium constants are given as empirical functions of ambient temperature and salinity (e.g., Weiss, 1974; Dickson and Goyet, 1994; Millero, 1995). The calcium carbonate formation is considered to be proportional to feeding of benthic fauna (suspension feeders and deposit feeders), and the calcium carbonate dissolution is formulated based on differences from the concentration of CO_3^{2-} calculated at each time step, to the saturated concentration of CO_3^{2-}. The saturated concentration of CO_3^{2-} is described as a function of ocean depth (Broecker and Takahashi, 1978). The formulations are described in Tables B6 and B7 in Appendix B.

All three systems comprise the benthic and pelagic coupled ecosystem and are sensitive to the vertical profiles at the microscale in the benthic system (i.e., dissolved oxygen concentration, ratio of oxic,

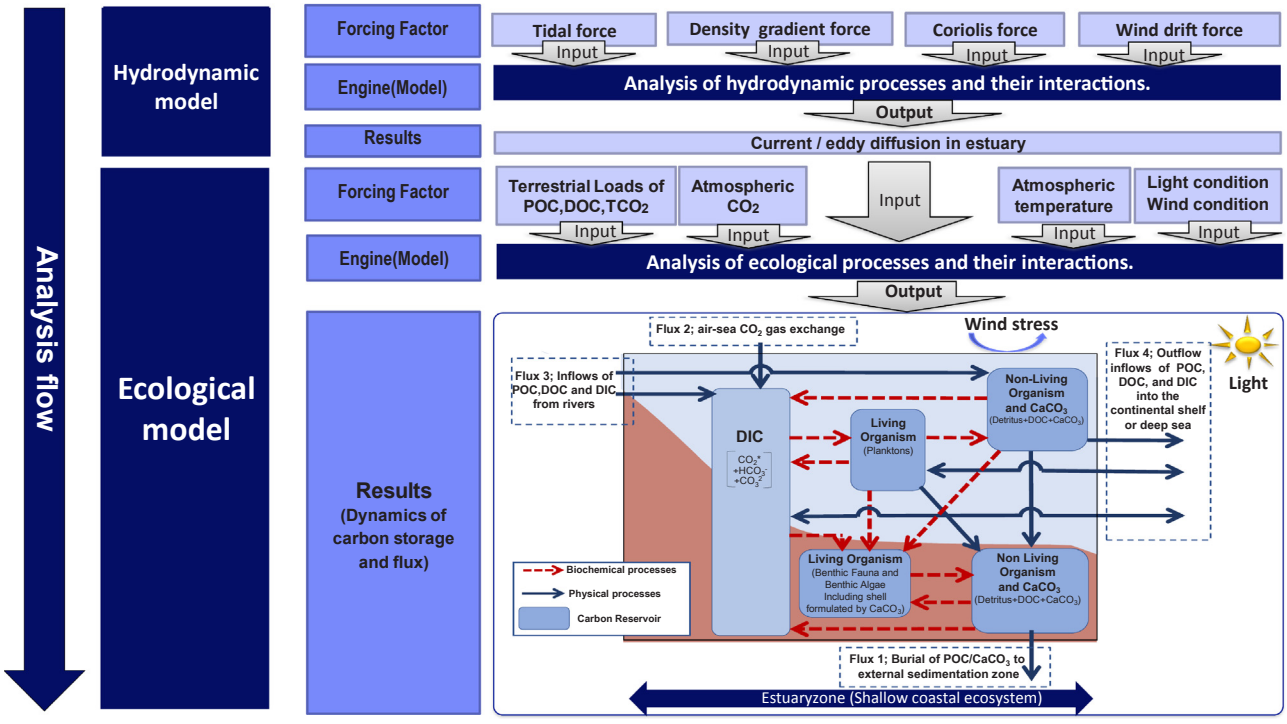

Fig. 2. Analysis Flow of EMAGIN-B.C. The flow field in the estuary is calculated from the hydrodynamic model driven by tidal forces, density gradients, the Coriolis force, and the wind-drift force. The output of the hydrodynamic model becomes the input data of the ecological model. Ecosystem dynamics calculated from the ecological model were driven by atmospheric temperature, light conditions, wind, carbon inflow from rivers, and atmospheric CO_2.

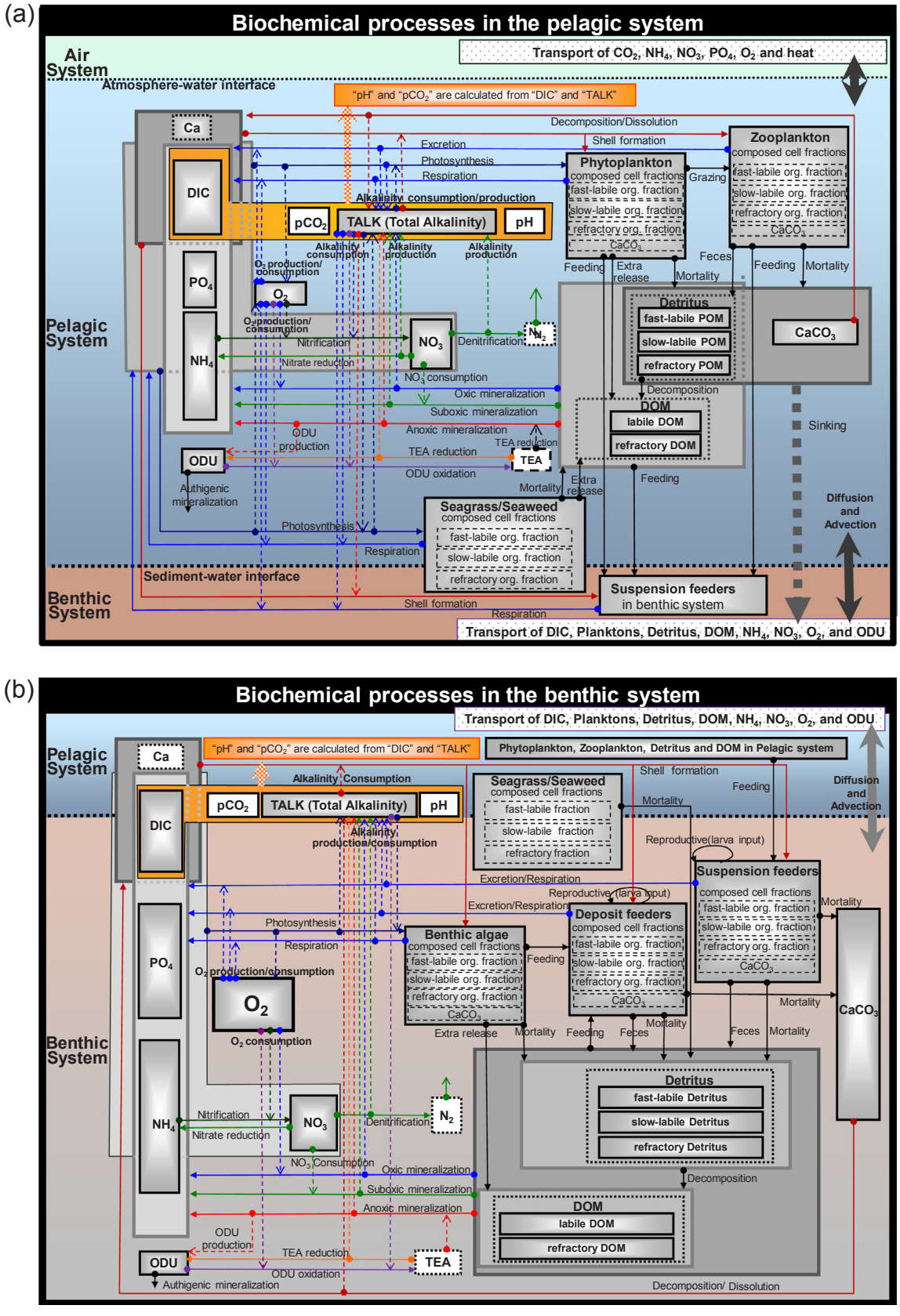

Fig. 3. (a), Model variables (boxes) and biochemical processes (arrows) in the pelagic system of EMAGIN-B.C. ver. 1.0. In Fig. 3(a), TALK is Total Alkalinity, ODU is Oxygen Demand Unit, and TEA is Terminal Electron Accepter. For stoichiometric relationships and units of TALK, ODU, and TEA, refer to Table 1, Appendix B, and Sohma et al., 2008. (b), Model variables (boxes) and biochemical processes (arrows) in the benthic system of EMAGIN-B.C. ver. 1.0. In Fig. 3(b), TALK is Total Alkalinity, ODU is Oxygen Demand Unit, and TEA is Terminal Electron Accepter. For stoichiometric relationships and units of TALK, ODU, and TEA, refer to Table 1, Appendix B, and Sohma et al., 2008.

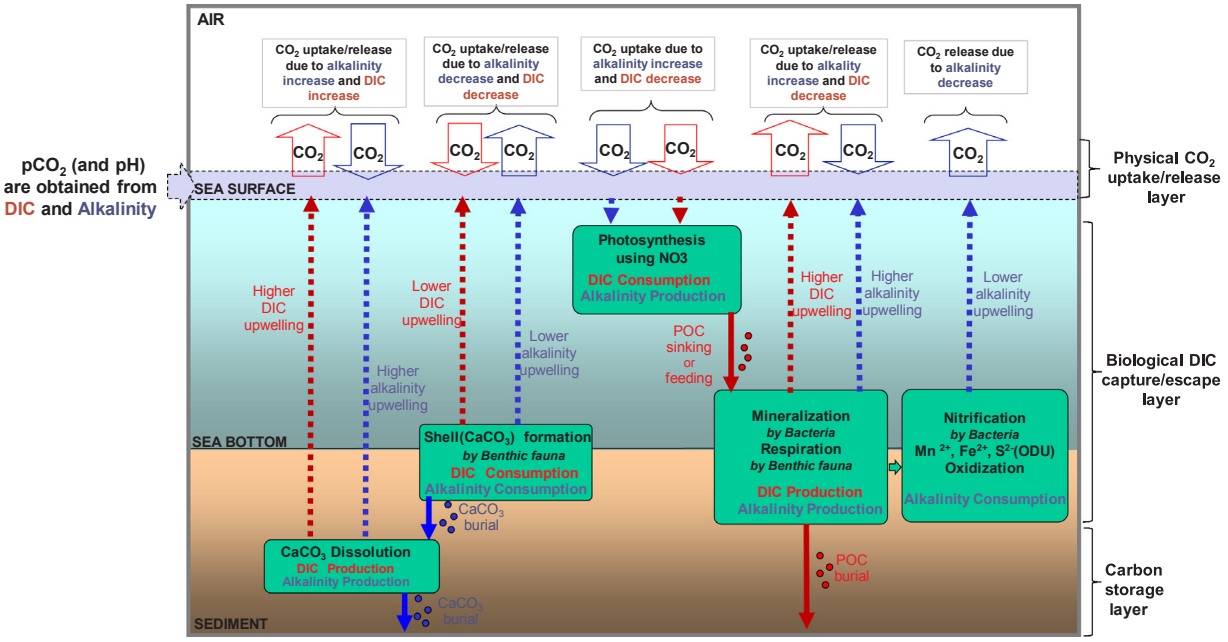

Fig. 4. The essential biochemical processes related to physical CO_2 uptake, biological DIC capture, and carbon storage in the shallow coastal area treated in EMAGIN-B.C. Red arrows describe DIC increase/decrease mechanisms. Blue arrows describe total alkalinity increase/decrease mechanisms. Physical CO_2 uptake/release mechanism is the function of differences in the CO_2 (pCO_2) pressure at the ocean surface. (Shell formations of phytoplankton and zooplankton in Fig. 3(a) are set at zero in shallow coastal areas of Japan).

Table 1
Stoichiometric relationships associated with biochemical processes and the production/consumption of DIC and total alkalinity (TALK) through the biochemical processes treated in EMAGIN-B.C.

Biochemical Processes	DIC production or consumption (ΔDIC)	Alkalinity production or consumption (ΔTALK)
Photosynthesis using NH_4-N $m\cdot(CO_2) + n\cdot(NH_3) + (H_3PO_4) + m\cdot(H_2O)$ $\rightarrow(CH_2O)_m(NH_3)_n(H_3PO_4) + m\cdot(O_2)$	−1 [molCO_2/molC]	(−n+1)/m [eq/molC]
Photosynthesis using NO_3-N $m\cdot(CO_2) + n\cdot(NO_3^-) + (H_3PO_4) + (m+n)\cdot(H_2O) + n\cdot H^+$ $\rightarrow(CH_2O)_m(NH_3)_n(H_3PO_4)+(2n+m)\cdot(O_2)$	−1 [molCO_2/molC]	(n+1)/m [eq/molC]
Oxic mineralization, Excretion of plankton and benthic fauna $(CH_2O)_m(NH_3)_n(H_3PO_4)+m\cdot(O_2)$ $\rightarrow m\cdot(CO_2) + n\cdot(NH_3^-) + (H_3PO_4) + m\cdot(H_2O)$	1 [molCO_2/molC]	(n-1)/m [eq/molC]
Suboxic mineralization $(CH_2O)_m(N^{\dagger}H_3)_n(H_3PO_4) + a\cdot(HN^{\ddagger}O_3)$ $\rightarrow m\cdot(CO_2) + a\cdot x/2\cdot(N_2^{\ddagger})$ $+ n\cdot(N^{\dagger}H_3) + a\cdot(1-x)\cdot(N^{\ddagger}H_3) + (H_3PO_4) + b\cdot(H_2O)$ where a = −4 m/(3x−8), b = m·(3x−4) / (3x−8), $0 \le x \le 1$, These condition satisfied $a \ge 0$ and $b \le 0$ at anytime	1 [molCO_2/molC]	(n+2 a-ax-1)/m [eq/molC]
Anoxic mineralization $(CH_2O)_m(NH_3)_n(H_3PO_4) + m\cdot(TEA)$ $\rightarrow m\cdot(CO_2) + n\cdot(N\,H_3) + (H_3PO_4) + m\cdot(ODU) + Q\cdot(H_2O)$ where, ODU = $2Mn^{2+}$, $4Fe^{2+}$, and $(1/2)S^{2-}$, TEA = $2MnO_2$, $2Fe_2O_3$, and $(1/2)SO_4^{2-}$	1 [molCO_2/molC]	(n-1 + 13/3 m)/m [eq/molC] (averaged value of reactions used each ODU matter)
Nitrification $NH_3+H_2O+2O_2 \rightarrow NO_3^- + 2H_2O + H^+$		−2 [eq/molN]
ODU oxidization $ODU + O_2 \rightarrow TEA$ where, ODU = $2Mn^{2+}$, $4Fe^{2+}$, and $(1/2)S^{2-}$, TEA = $2MnO_2$, $2Fe_2O_3$, and $(1/2)SO_4^{2-}$		13/3 [eq/molODU] (averaged value of reactions used each ODU matter)
Production of calcium carbonate (shell formation of plankton, benthic algae, and benthic fauna) $Ca^{2+} + CO_3^{2-} \rightarrow CaCO_3$	−1 [molCO_2/molC]	−2 [eq/molCa]
Dissolution of calcium carbonate $CaCO_3 \rightarrow Ca^{2+} + CO_3^{2-}$	1 [molCO_2/molC]	2 [eq/molCa]

*1) Benthic fauna represents suspension feeders and deposit feeders in Fig. 2.
*2) ODU means Oxygen Demand Unit and TEA is Terminal Electron Accepter. For stoichiometric relationships and units of TALK, TEA, and ODU, refer to Appendix B and Sohma et al., 2008.
*3) m, n denote C, N, P ratio of created or mineralized organic matter. i.e., C:N:P = m:n:1.
*4) x denotes the ratio of nitrogen reducing to nitrogen gas ($N_2^{\ddagger}$) and reducing to ammonium from nitrate by suboxic mineralization. i.e., $N_2^{\ddagger}$:$N^{\ddagger}H_3$ = x:(1−x).
*5) a, b are coefficients determined from the stoichiometric relationship.

suboxic, and anoxic mineralization, nitrification, and Mn^{2+}, Fe^{2-}, and S^{2-} (ODU) oxidization). EMAGIN-B.C. describes the processes in Fig. 4, via the benthic and pelagic coupled system, and describes the vertical micro profiles of the biogeochemical processes in the benthic system.

3. Implementation

EMAGIN-B.C. was applied to Tokyo Bay and was used to calculate the daily and seasonal dynamics of the average year, i.e., the ecological dynamics in a year-long period called the "annual periodical steady state of the existing Tokyo Bay." The implementation method is almost identical to that in Sohma et al. (2008). Therefore, we summarize the explanation here and discuss the new components of the implementation.

The prescribed functions (forcing functions) of the hydrodynamic and ecological models (i.e., freshwater, nutrients, and carbon input from rivers, meteorological conditions (e.g., light intensity, wind), and open boundary conditions of model variables) were set as one-year periodic functions based on data observed from 1998 to 2002. The convergence state of this simulation describes the dynamics in a one-year period. The horizontal spatial resolution for the simulation is different from those in the hydrodynamic and ecological models. In the hydrodynamic model, a 2 × 2 km grid was implemented, whereas, in the ecological model, the Tokyo Bay area under consideration was divided into 26 zones (boxes) (Fig. 5). The input data for the ecological model from the hydrodynamic model (e.g., flow velocity, eddy viscosity, and temperature) were averaged spatially and adjusted to the 26 boxes of the ecological model while respecting the flow continuity equation of water volume. The vertical grid interval in the benthic system was set to 0.1–12 mm, and the vertical spatial resolution in the pelagic system was set at 1–2 m. Furthermore, the time step was set at 0.2 h, enabling the demonstration of both daily and seasonal dynamics. For the biochemical and physical parameters, values were set within range of or at the same order as the field/experimental data or the data used in other models. The parameter values set in this study are listed in Appendix D.

4. Validation

The model was validated by confirming the reproducibility of the spatiotemporal dynamics of the ecosystem through a comparison between the observed data and the model outputs. The outputs are the result of the self-sustained ecological connectivity among biochemical-physical processes in the benthic and pelagic systems. Therefore, reproduction with all model variables is difficult, however, if it succeeds, it will be strong evidence that the model closely approximates the real ecosystem and its mechanisms. Samples of the seasonal dynamics of the model outputs concerned with the carbonate chemistry system (i.e., DIC, TALK, pCO_2, and pH) are shown in Fig. 6. In the zones where observed data exist, the data are plotted in Fig. 4 simultaneously. In addition, Pearson's correlation coefficient (R) between the observed and calculated values, the P-values (P), and the sample number (N) of the observed data are shown in Table 2. As shown in Fig. 6 and Table 2, the model has been mostly successful in reproducing the observed values in the model variables with carbonate chemistry except for the pH of the bottom layer at (i, j) = (3, 5), whose correlation coefficient R is 0.17 (P = 0.463) and whose P-value is the highest among the variables. However, except for the data on 1 August, 1 September, and 3 September, the correlation coefficient of the pH of the bottom layer is 0.62 (P = 0.008), and its reliability increases. The reproducibility of the seasonal variations, daily variations, and spatial distributions of the model variables (e.g., phytoplankton, detritus, DOM, nutrients, dissolved oxygen, benthic algae, and benthic fauna) concerned with the carbon-nutrients-oxygen cycling system and the food-web system is at the same level as that of the carbonate chemistry system (i.e., DIC, pCO_2, and pH; refer to Appendix E).

5. Sample of the model output: carbon budget in Tokyo Bay

In this section, the model results of the annual average of the carbon budget, including CO_2 physical uptake, DIC biological capture, and the carbon storage functions in Tokyo Bay, are introduced as output examples using the validated EMAGIN-B.C.

In Fig. 7 -left, the carbon cycle for all of Tokyo Bay (the entire calculation area in Fig. 5) in spring (May), summer (August), autumn (November), and winter (February) are shown. Fig. 7-right shows the vertical profile of the DIC production/consumption due to biochemical processes and the air-sea CO_2 gas exchange (physical CO_2 uptake flux in Fig. 1) and the burial flux into deeper sediment (carbon storage flux in Fig. 1) at zone (ij) = (5, 4). Table 3 shows the breakdown of biochemical and physical fluxes, which summarizes the fluxes described in Fig. 7-left. As for the physical CO_2 uptake flux and the carbon storage flux, Fig. 7-right shows that the carbon storage flux remains mostly stable in all seasons. In

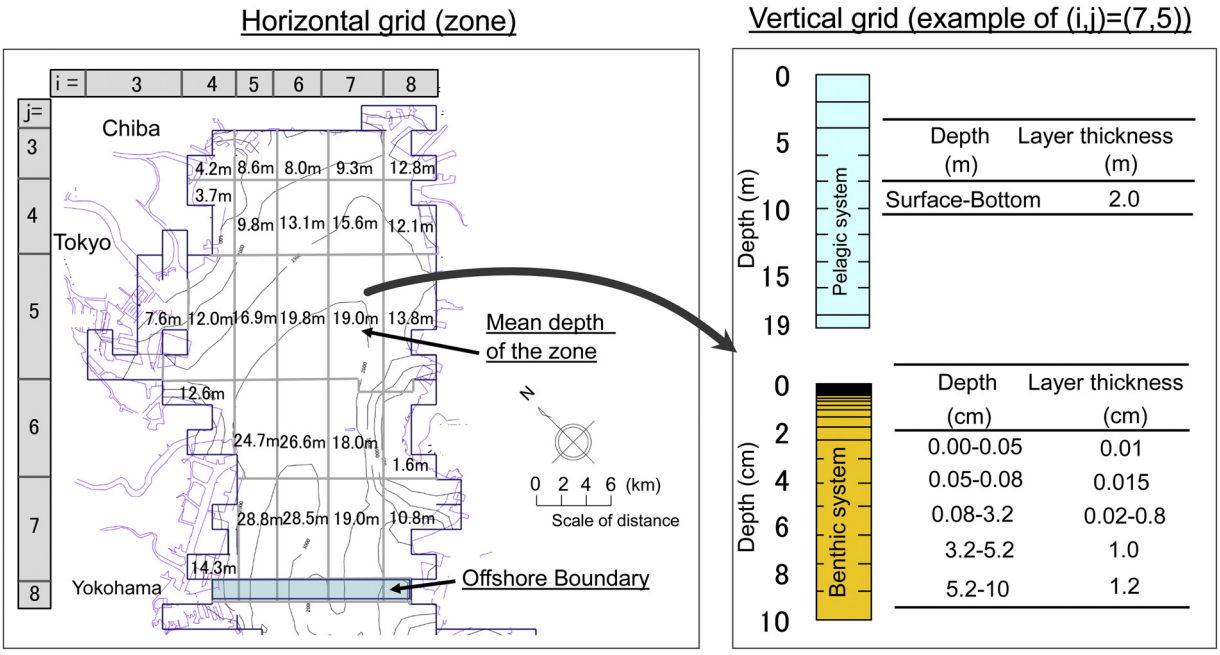

Fig. 5. Geographical description of Tokyo Bay (calculated area, spatial resolution in the vertical and horizontal directions, and the coordinated zone; (ij) on the model application). The numbers denoted at each zone are the mean depth of the zone (revised from Sohma et al., 2008). The left-side box shows the horizontal grid (zone). The right-side box shows the vertical grid and its example at (i, j) = (7, 5).

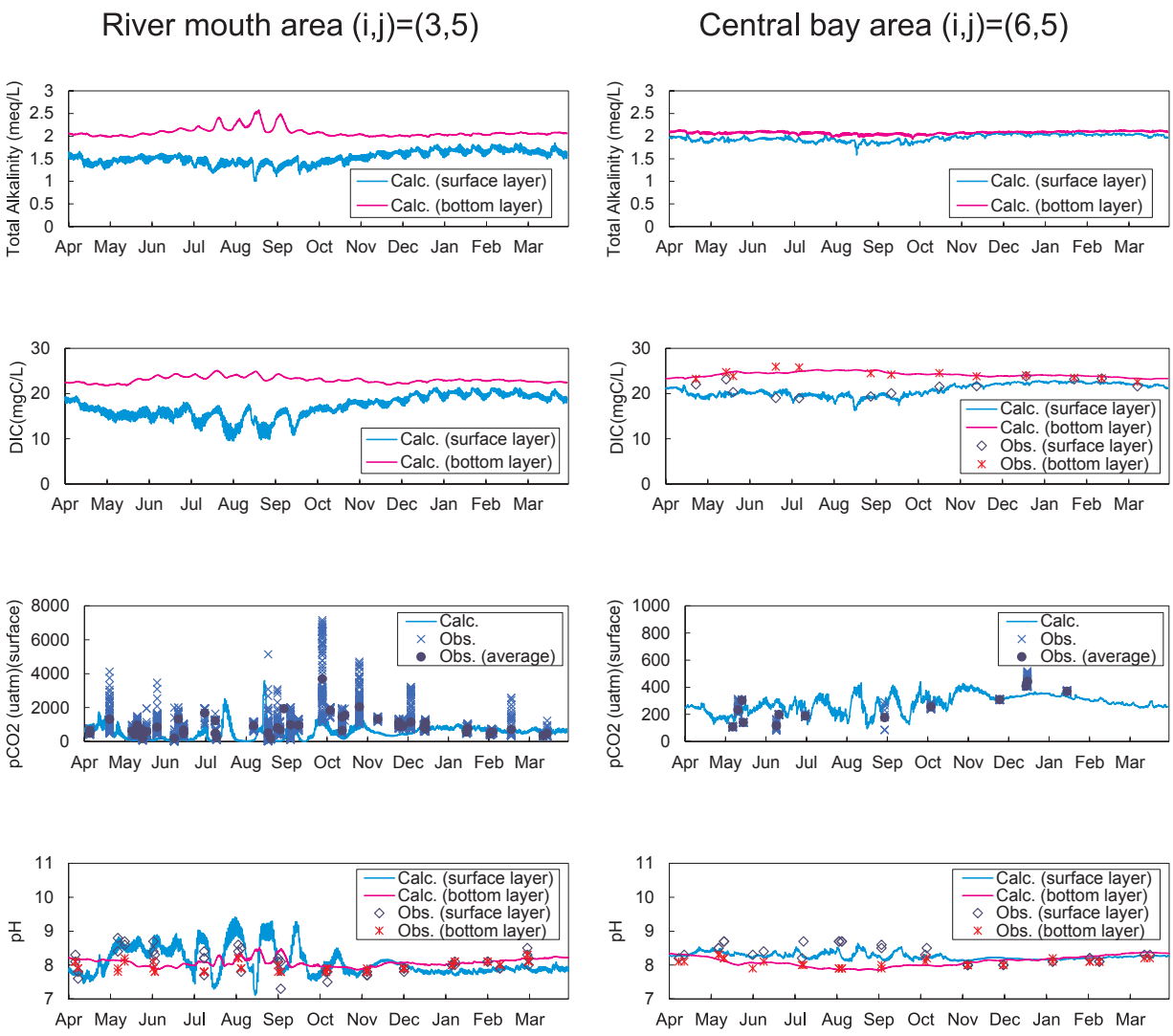

Fig. 6. Seasonal variations in Total Alkalinity (TALK), DIC, pCO_2, and pH in zones (i,j) = (3,5) and (6,5). Comparison between the observed data (dots) and model outputs (lines). The location of the area (i, j) is described in Fig. 5.

Table 2
The results of statistical analysis (Pearson's correlation analysis) between the observed and calculated values at zones (i, *j*) = (3, 5) and (6, 5).

(a) at zone (i, j) = (3, 5)

Model variable		Correlation coefficient : R	P value : P	Sample number : N
DIC	surface layer	–	–	–
	bottom layer	–	–	–
pCO_2		0.42	0.002	51
pH	surface layer	0.61	0.004	21
	bottom layer	0.17	0.463	21
		0.62*	0.008*	18*
			(* except for three data points on Aug. 1, Sep. 1 and Sep. 3)	

(b) at zone (i, j) = (6, 5)

Model variable		Correlation coefficient : R	P value : P	Sample number : N
DIC	surface layer	0.68	0.010	13
	bottom layer	0.78	0.002	13
pCO_2		0.65	0.017	13
pH	surface layer	0.46	0.039	20
	bottom layer	0.62	0.003	20

*1) R is Pearson's correlation coefficient between the observed and calculated values. P is P-value.
*2) The lower the P-value, the more likely it is that the observed value was reproduced/explained by the calculated value (For example, R = 0.68, P = 0.01 means that the probability that R = 0.68 is 1%, despite no correlation.).

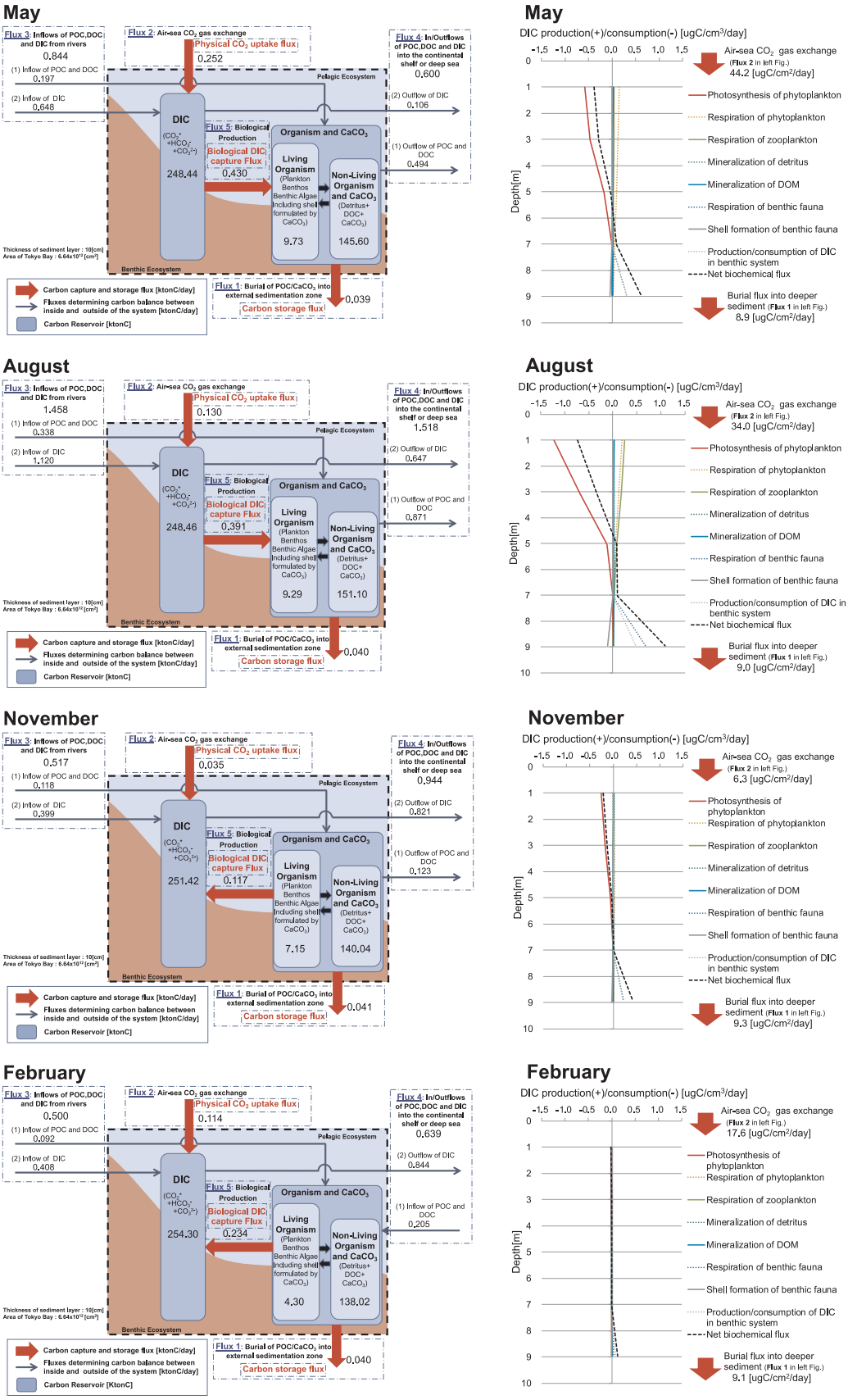

Fig. 7. Figures on the left are seasonal variations of the carbon cycle throughout Tokyo Bay (the whole calculation area) and those on the right are the vertical profiles of DIC production and consumption due to biochemical processes at zone (i, j) = (5, 4). The calculated Tokyo Bay area is 664 km^2.

Table 3
The details of the biochemical and physical fluxes (contents) that summarize the fluxes described in Figs. 7 and 8.

Category	Notation in Figs. 7 and 8	Contents
Carbon Reservoir	DIC	Total CO_2 composed of $CO_2^* + HCO_3^- + CO_3^{2-}$
	Living Organism	Phytoplankton, Zooplankton, Benthic algae, Suspension feeder, Deposit feeder (including shell formulated by $CaCO_3$)
	Non Living Organism and $CaCO_3$	Detritus, Dissolved Organic Carbon (DOC), $CaCO_3$ both in the benthic and pelagic systems
Fluxes existing between the inside and outside of the system	Flux 1	Burial of Detritus + DOC + $CaCO_3$ to external sedimentation zone
	Flux 2	Air-sea CO_2 gas exchange
	Flux 3(1)	Inflows of DIC from rivers
	Flux 3(2)	Inflows of POC (Planktons and Detritus) and DOC from rivers
	Flux 4(1)	In/outflow into the continental shelf of DIC
	Flux 4(2)	In/outflow into the continental shelf of POC and DOC
	Flux 5	Net biological processes of phytoplankton, zooplankton, benthic algae, benthic fauna (suspension feeders, deposit feeders) and bacteria. i.e, [photosynthesis of phytoplankton and benthic algae], [excresion of phytoplankton, zooplankton, benthic faunas], [mineralization of detritus and dissoloved organic matter] and [shell formation of suspension feeders, $CaCO_3$ dissolution].

contrast, the physical CO_2 uptake flux varies by about eight (0.252/0.035) times depending on the season. This is because the carbon storage flux is largely dominated by the burial of refractory detritus and $CaCO_3$ that were accumulated in deeper sediments over the past 10- to 100-year timescale. Therefore, daily fluctuations in the pelagic ecosystem or climatic conditions have lower impacts on the burial flux compared to the air-sea CO_2 gas exchange. For the biochemical process, Fig. 7-left shows that biological DIC capture flux (i.e., the net biological production from DIC to organisms and $CaCO_3$) is highest in spring and lowest (negative value) in winter. In addition, Fig. 7-right shows that DIC production occurs mainly at the sediment or sediment-water interface, and the DIC production is derived from the mineralization of the benthic detritus and respiration of benthic fauna. From the viewpoint of the vertical integral value at zone (i, j) = (5, 4), DIC consumption is larger than DIC production biochemically in the spring and summer seasons. Incidentally, in the model, the shell formation of $CaCO_3$ is mainly due to the growth of bivalves (suspension feeders) in shallow areas. As for the carbon inflows of river origins and the carbon outflows offshore of Tokyo Bay, the carbon flowing into Tokyo Bay through rivers is largest in the summer. Concerning the amount of carbon transported outside of Tokyo Bay at the offshore boundary, the total amount of organic carbon (POC and DOC) and dissolved inorganic carbon (DIC) carried away is also largest in the summer. However, with respect to DIC (i.e., Flux 4 (2) in Fig. 7-left), a larger amount is transported outside the bay in winter and autumn than in summer. In addition, a minimum amount of DIC is transported outside the bay in the spring, although the DIC inflow from the river in spring is the second largest among all the seasons. These results indicate that the summer and spring ecosystems of Tokyo Bay have a higher biological DIC capture function than do autumn and winter. During the winter, organic carbon (POC and DOC) is brought into Tokyo Bay. This phenomenon results from lower POC and DOC concentrations on the inside compared to the outside of Tokyo Bay, which is attributed to the low biological production (i.e., low biological DIC capture flux) inside Tokyo Bay. Previous studies on Tokyo Bay revealed part of the carbon flow and the amount of benthic organic matter in the entire carbon cycle, based on observational data (Kubo and Kanda, 2017; Ogawa and Ogura, 1997; Sato et al., 2006). In addition, there have been cases in which the annual average value of the carbon balance has been analyzed by the carbon budget model (Yanagi et al., 1993). However, the analysis by EMAGIN-B.C. presented herein quantitatively shows the relationship between the detailed biological/chemical/physical processes and the resultant seasonal variations in the carbon cycle for the first time.

Fig. 8 -left shows the annual averaged carbon cycle (one-year carbon budget) throughout the Tokyo Bay (the entire calculation area), and Fig. 8-right shows the vertical profile of the annual averaged DIC production/consumption biochemically and the air-sea CO_2 gas exchange as well as the burial flux into the deeper sediments at zone (i, j) = (5, 4). As shown in Section 3, since the model simulation calculates an annual cycle steady state that returns to the same model variable values on a one-year cycle, the sum of carbon inflows/outflows between the Tokyo Bay area and its outside area described by this calculation is zero (i.e., steady state) in Fig. 8 -left. In the one-year carbon budget, **96.1%** of the total carbon flowing into Tokyo Bay from the atmosphere and river flows out to the offshore area (outside of Tokyo bay), (i.e., Flux 4 / {Flux 2 + Flux 3} in Fig. 8-left), and **3.9%** is stored in deeper sediment layer (i.e., Flux 1 / {Flux 2 + Flux 3} in Fig. 8-left). In addition, **81.6%** of the DIC flowing into the Tokyo Bay from the atmosphere and river flows out to the offshore area as DIC (i.e., Flux 4(2) / {Flux 2 + Flux 3(2)} in Fig. 8-left) and **16.6%** of the DIC flowing into the Tokyo Bay from the atmosphere and rivers is temporally captured as

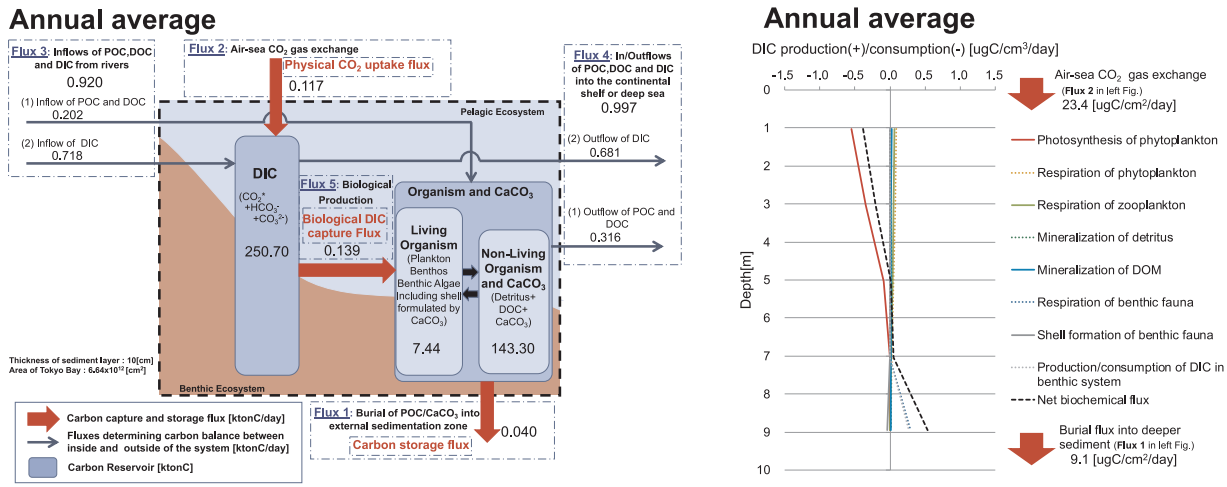

Fig. 8. Annual averaged carbon cycle throughout Tokyo Bay (the whole calculation area) and the vertical profile of DIC production and consumption at zone (i, j) = (5, 4). The calculated Tokyo Bay area is 664 km^2.

organic matter and $CaCO_3$ by biological DIC capture flux (i.e., Flux 5 / {Flux 2 + Flux 3(2)}). These results indicate that Tokyo Bay captures DIC from rivers and CO_2 from the atmosphere as organic carbon and $CaCO_3$ in Tokyo Bay and stores carbon by burial of POC and$CaCO_3$. These results suggest that the Tokyo Bay system could sequester a small percentage of the carbon entering the system. When considering a snapshot of the system at a single level, this may not sound like much, but it is not insignificant. However, at larger or even global scales or as a result of time, either the loss or remediation of tidal flats/estuaries could have a non-negligible impact on climate change. This model has the potential to reveal/estimate/predict its impact and system mechanisms by (1) analyzing the patterns and variability of the carbon stock and flow described in the model from a more diversified perspective and (2) pursuing the key processes and interactions through sensitivity analysis. In addition, the model has the potential to be both a communication platform among scientists as well as among scientists and policymakers since the model is based on processes and makes it possible to explain the causes of carbon dynamics. The model introduced herein is the basis for these future projects

6. Conclusion

The final goal of the EMAGIN-B.C. Project is to reveal the CO_2 physical uptake, DIC biological capture, and carbon storage function on the basis of biogeochemical and physical processes and to estimate and predict the climate change mitigation function of all types of shallow coastal ecosystems with high biological productivity. As a first step, we developed an ecosystem model, EMAGIN-B.C. ver 1.0, applicable to "eutrophic enclosed urbanized waters with river inflow," where many observed data exist and is relatively less complex compared to other high biological productive coastal areas (i.e., mangroves, coral reefs, and salt marshes).

EMAGIN-B.C. ver 1.0 is a new model that possesses the features described below:

- For demonstrating the series of processes in which carbon is captured in water or sediment surfaces and is stored into deeper sediments, the model is composed of benthic and pelagic ecosystems.
- For estimating the carbon capture function associated with grazing at the trophic level, the model describes the food web among detritus, phytoplankton, zooplankton, and benthic fauna.
- For estimating the air-sea CO_2 gas exchange, the model incorporates the carbonic chemistry theory among DIC, total alkalinity, pH, and pCO_2 as well as describes alkalinity production/consumption through biochemical processes in detail.
- For estimating the primary production affecting the biological DIC capture functions, the model considers Carbon-Nitrogen-Phosphorus-Oxygen-Calcium coupled cycles.
- For demonstrating (a) the effect of hypoxia on benthic fauna that affect the biological DIC capture functions and (b) the oxic, suboxic, and anoxic mineralization and re-oxidation of the Oxygen Demand Unit (ODU, comprised of Mn^{2+}, Fe^{2+}, and S^{2-}; Soetaert et al., 1996), which affect the alkalinity production, the model describes the vertical profiles of biochemical processes at the microscale (mm-scale pitch) in the sediments related to oxygen consumption/production.
- For estimating the carbon transport in the estuary and at the offshore boundary, the model was integrated with the hydrodynamic model.

EMAGIN-B.C. ver 1.0 was applied to Tokyo Bay and validated by the reproducibility of the seasonal ecosystem variations with observed and calculated values. Using the validated model, we analyzed the carbon budget, including CO_2 uptake, DIC capture, and the carbon storage functions in Tokyo Bay, obtaining the following results. Firstly, the dynamics of the air-sea CO_2 gas exchange flux changed greatly on a seasonal time scale. However, the buried carbon flux in deeper sediments was fairly stable. Secondly, in the summer, a high amount of DIC was transported to Tokyo Bay from the atmosphere and river and was stored in Tokyo Bay as organic carbon or calcium carbonate by high biological production activities. Thirdly, in the winter, DIC consumption due to biological production was low, and DIC production due to mineralization of organic matter occurred, although it was relatively lower than in the summer. As a result, more DIC flowed out to the offshore area than was transported/originated from the atmosphere and river. Finally, in terms of the annual carbon budget, Tokyo Bay incorporated inorganic and organic carbon from the river and absorbed CO_2 from the atmosphere. Then, of the incorporated and absorbed carbon, **3.9%** was stored in the benthic permanent sedimentary layer, and **96.1%** was transported to the offshore area of Tokyo Bay. The stored DIC as the organic carbon or the calcium carbonate formed by biological productivity was **16.6%** of DIC from the rivers and air-sea CO_2 gas exchange. **81.6%** of DIC flowing into Tokyo Bay from the atmosphere and river flowed out to the offshore area.

This paper highlighted various components of a specific model: (1) the model concept (clarification of the viewpoint of the model), (2) the numerical construction and its linkage with the model concept, and (3) the model demonstration applied to Tokyo Bay to check the model's reliability and the possibility of analyzing patterns and variability that might reveal the processes and interactions for carbon management. As shown in this paper, EMAGIN-B.C. can be a powerful tool to (1) predict/estimate the patterns and variability of CO_2 uptake, DIC capture, and carbon storage capacity of the estuary, (2) understand the processes and interactions that dominate the carbon balance in the estuary, and (3) be used for management as the communication platform among scientists and policymakers in efforts made toward climate change mitigation. In addition, by extending the applied area of the model to other shallow coastal areas (mangroves, coral reefs, salt marshes, seagrass beds, reef seaweed beds, and fjords), the climate change mitigation functions of those areas on a global scale would be possible to estimate/predict. As for Tokyo Bay, we predict future (1) analyses of its patterns and variability from a more diversified perspective of carbon stock and flow, (2) sensitivity analyses for pursuing the key processes and interactions and predicting future scenarios, and (3) extension of the applied area of the model. We also foresee a more extensive model development for application to other shallow coastal areas using EMAGIN-B.C. ver. 1.0. as the basis for future work.

Acknowledgements

We thank Yasuyuki Sekiguchi for his support in model development and analysis. We also thank reviewers for their valuable comments. This study was supported in part by a Canon Foundation Grant, by the research project on Accounting Rules of CO2 Sequestration for Creation of National GHG Inventories (ARCS) funded by Japan's Ministry of Economy, Trade and Industry and by JSPS KAKENHI Grant Numbers 18K04409 and 18H04156. A.S. and T.K. designed the research project. A.S. designed the model concept and construction and developed the model. A.S and H.S. performed the model analysis. A.S., F.N., and H.S. analyzed the model output. A.K. performed the field observation. A.S. wrote the paper.

Appendix A. Governing Equations and Assumptions

The following seven equations and four assumptions are applied in the ecological model.

(1) Equation for the pelagic system:

$$\frac{\partial C_w}{\partial t} = -(\boldsymbol{v_w} \bullet \nabla) C_w + \nabla \bullet (\boldsymbol{K} \bullet \nabla C_w) + \sum R \tag{A1}$$

where C_w = the model variables in the pelagic system, i.e., phytoplankton, zooplankton, detritus (fast labile detritus, slow labile detritus, refractory

detritus), dissolved organic matter (labile DOM, refractory DOM), DIC, TALK, NH_4-N, NO_3-N, PO_4-P, DO, and ODU [mass/L^3–liquid]; $\mathbf{v}_w$ = (u_w, v_w, w_w) = the flow velocity that already has been calculated by the hydrodynamic model [L/T]; t = time [T]; x, y, z = space coordinates [L]; ΣR = biochemical reactions and fluxes from outside the system [mass/L^3–liquid/T];and $\mathbf{K}$ = the eddy diffusion (viscosity) tensor [L^2–liquid/T].
(2) Diagenetic equation for benthic dissolved substances:

$$\frac{\partial(\phi C)}{\partial t} = \frac{\partial\left\{D_B\frac{\partial(\phi C)}{\partial z} + \phi\,(D_S + D_I + D'_B)\frac{\partial C}{\partial z}\right\}}{\partial z} + \phi\alpha(C_0 - C) - \frac{\partial(\phi\, vC)}{\partial z} + \phi R_{ads} + \phi\sum R' \tag{A2}$$

where φ = porosity [–]; C = the model variables of the dissolved substances in the benthic system, i.e., dissolved organic matter (labile DOM, refractory DOM), NH_4-N, NO_3-N, PO_4-P, DO, and ODU [mass/L^3–liquid]; C_0 = concentration of dissolved substances at sediment-water interface [mass/L^3–liquid]; D_S = molecular diffusion coefficient in sediment including the effects of tortuosity [L^2–sediment/T]; D_B = solid bio-diffusion coefficient (interphase mixing expression) [L^2–sediment/T]; D'_B = solid bio-diffusion coefficient (interphase mixing expression) [L^2–sediment/T]; D_I = irrigation coefficient (diffusion-like expression) [L^2–sediment/T]; α = irrigation coefficient2 [1/T]; v = velocity of burial of water below the sediment-water interface [L–sediment/T]; R_{ads} = reactions of dissolved materials due to equilibrium adsorption or desorption [mass/L^3–liquid/T]; and $\Sigma R'$ = all other slow (irreversible) biochemical reactions [mass/L^3–liquid/T].
(3) Diagenetic equation for benthic particulate substances:

$$\frac{\partial\{(1-\varphi)\overline{\rho_s}\,\overline{C}\}}{\partial t} = \frac{\partial\left[D_B\frac{\partial\{(1-\varphi)\overline{\rho_s}\,\overline{C}\}}{\partial z}\right]}{\partial z} + \frac{\partial\left[D'_B(1-\varphi)\overline{\rho_s}\frac{\partial\overline{C}}{\partial z}\right]}{\partial z} - \frac{\partial[D'_B(1-\varphi)\overline{\rho_s}w\overline{C}]}{\partial z} + (1-\varphi)\overline{\rho_s}\,\overline{R_{ads}} + (1-\varphi)\overline{\rho_s}\sum\overline{R'} \tag{A3}$$

where $\overline{C}$ = the concentration of a particulate substance in terms of mass per unit mass of total solids, i.e., detritus (fast labile detritus, slow labile detritus, refractory detritus), absorbed DOM, and absorbed NH_4-N; $\overline{\rho_s}$ = density of total solid phase [mass-solid/ L^3–solid]; w = rate of depositional burial of solids [L–sediment/T]; $\overline{R_{ads}}$ = reactions of dissolved materials due to equilibrium adsorption or desorption [mass/mass-solid/T]; and $\sum\overline{R'}$ = all non-equilibrium slow biochemical reactions [mass/mass-solid/T].
(4) Equations for suspension feeders, deposit feeders, benthic algae, and $CaCO_3$:

$$\frac{\partial B}{\partial t} = \sum R_B \tag{A4}$$

where B = mass, expressed per square of sediment [mass/L^2–sediment] and R_B = biochemical reactions [mass/L^2–sediment].
(5) Equation for the relation of the adsorption-desorption reaction:

$$\overline{R_{ads}} = \frac{-\varphi}{(1-\varphi)\overline{\rho_s}}R_{ads} \tag{A5}$$

(6) Equation for the mass/volume conservation of the benthic solid phase:

$$\frac{\partial\varphi}{\partial t} + \frac{\partial(v\cdot\varphi)}{\partial z} = \frac{\partial}{\partial z}\left(D_B\frac{\partial\varphi}{\partial z}\right) \tag{A6}$$

(7) Equation for the mass/volume conservation of the benthic liquid phase:

$$\frac{\partial(1-\varphi)}{\partial t} + \frac{\partial(w\cdot(1-\varphi))}{\partial z} = \frac{\partial}{\partial z}\left(D_B\frac{\partial(1-\varphi)}{\partial z}\right) \tag{A7}$$

Note that w and v in the benthic system are calculated to meet the relationship between Eqs. (A6) and (A7).
The following assumptions are imposed on the equations described above (Berner, 1980):
i. Seawater is treated as an incompressible liquid: $div\ \mathrm{v_w} = 0$
ii. The density of a solid does not change with space or time: $\overline{\rho_s}$ is constant
iii. The equilibrium expression for simple linear adsorption: $\overline{C} = K'C$, K' = adsorption coefficient.
iv. The adsorptive property does not change with space or time: K' is constant.
v. If $\overline{C}$ is adsorbed substances, then there are no slow diagenetic reactions, hence, $\sum\overline{R'} = 0$ in Eq. (A3).

Appendix B. Formulations of major biochemical processes

The details of the model variables and formulations of biochemical processes are shown in Tables B1–B7.

Table B1
Notation of model variables (pelagic system).

Model variable	Unit	Notation and [No.] in the model
Phytoplankton	mgC/l (μgC/ml)	PP [01]
Zooplankton	mgC/l (μgC/ml)	ZP [02]
Fast labile detritus	mgC/l (μgC/ml)	WDE_1 [03,1]
Slow labile detritus	mgC/l (μgC/ml)	WDE_2 [03,2]
Refractory detritus	mgC/l (μgC/ml)	WDE_3 [03,3]
Labile dissolved organic matter (Labile DOM)	mgC/l (μgC/ml)	WDM_1 [04,1]
Refractory dissolved organic matter (Refractory DOM)	mgC/l (μgC/ml)	WDM_2 [04,2]
Ammonium (NH_4)	mgN/l (μgN/ml)	WNX [05]
Nitrate (NO_3)	mgN/l (μgN/ml)	WNY [06]
Phosphate (PO_4)	mgP/l (μgP/ml)	WDP [07]
Reduced substances (ODU; i.e., Fe^{2+}, Mn^{2+}, S^{2-})	mg/l (μg/ml)	WOU [08]
Dissolved oxygen	mg/l (μg/ml)	WDO [09]

(continued on next page)

Table B1 (*continued*)

Model variable	Unit	Notation and [No.] in the model
DIC (Total CO_2)	mgC/l (μgC/ml)	WTC [10]
Calcium carbonate ($CaCO_3$)	mgC/l (μgC/ml)	WCC [11]
Total alkalinity (TALK)	(meq/l) μeq/ml	WAL [12]
pH	–	WPH [13]
Partial pressure of CO_2 (pCO_2)	μatm	WPS [14]
HCO_3^-	mgC/l (μgC/ml)	WCY [15]
CO_3^{2-}	mgC/l (μgC/ml)	WCZ [16]
CO_2^*; i.e., Sum of $CO_{2,aq}$ and H_2CO_3	mgC/l (μgC/ml)	WCX [17]

*1) TEA [mg/l] and N_2 [mgN/l] in Fig. 3(a) are not treated as model variables.

Table B2
Notation of model variables (benthic system).

Model variable	Unit	Notation and [No.] in the model
Suspension feeders	μgC/cm^2 sediment	SFB [51]
Deposit feeders	μgC/cm^2 sediment	DFB [52]
Fast labile detritus	μgC/cm^3 solid	DET_1 [53,1]
Slow labile detritus	μgC/cm^3 solid	DET_2 [53,2]
Refractory detritus	μgC/cm^3 solid	DET_3 [53,3]
Labile dissolved organic matter	mgC/l (μgC/ml)	DOM_1 [54,1]
Refractory dissolved organic matter	mgC/l (μgC/ml)	DOM_2 [54,2]
Ammonium	mgN/l (μgN/ml)	HNX [55]
Nitrate	mgN/l (μgN/ml)	HNY [56]
Phosphate	mgP/l (μgP/ml)	DIP [57]
Reduced substances (ODU; i.e., Fe^{2+}, Mn^{2+}, S^{2-})	mg/l (μg /ml)	ODU [58]
Dissolved oxygen	mg/l (μg/ml)	DOO [59]
Benthic algae	μgC/cm^2 sediment	BAL [60]
Seagrass	μgC/cm^2 sediment	SGS [61]
Seaweed	μgC/cm^2 sediment	SWD[62]
Calcium carbonate ($CaCO_3$)	μgC/cm^2 sediment	CAC [63]

*1) TEA [mg/l] and N_2 [mgN/l] in Fig. 3(b) are not treated as model variables.

Table B3
General variables and prescribed functions in the model.

General Variables and Prescribed Functions	Unit	Description
z	cm	Water depth or sediment depth
Δz	cm	Thickness of layer
dt	h	Calculation time step
φ	–	Porosity
$\overline{\rho_s}$	g/cm^3	Density of sediment
TempW, TempB	˚C	Temperature of sea water and sediment
I_0, I_B	μE/m^2/s	Light intensity on sea surface and sediment surface

Table B4
Ratio and distribution functions (prescribed function or calculated in the model).

Functions	Description
$R_{FOD51,1}$, $R_{FOD51,2}$, $R_{FOD51,3}$	Composition ratio (ratio of fast-labile, slow-labile, and refractory/very slow-labile part) of prey of suspension feeders
$R_{ncFOD51}$, $R_{pcFOD51}$	N/C, P/C ratio of prey of suspension feeders
R_{Zfec51}, R_{Zexc51}, R_{Zmor51}	Vertical distribution of faces, excretion, and mortality of suspension feeders
$R_{FOD52,1}$, $R_{FOD52,2}$, $R_{FOD52,3}$, $R_{FOD52,541}$, $R_{FOD52,542}$	Composition ratio (ratio of fast-labile, slow-labile, and refractory/very slow-labile part) of prey of deposit feeders
$R_{ncFOD52}$, $R_{pcFOD52}$	N/C, P/C ratio of prey of deposit feeders
R_{Zfee52}, R_{Zfec52}, R_{Zexc52}, R_{Zmor52}	Vertical distribution of feeding, feces, excretion, and mortality of deposit feeders
R_{Zpho60}, R_{Zres60}, R_{Zmor60}	Vertical distribution of photosynthesis, base respiration, and mortality of benthic algae
$R_{FOD52,60}$	Ratio of benthic algae to prey of deposit feeders

Table B5
Dissociation constant for the carbon dioxide system.

Functions	Description	Major Source *1)
K_0	The solubility coefficient of carbon dioxide in seawater	1
K_1	The first dissociation constant of carbonic acid	1
K_2	The second dissociation constant of carbonic acid	1

*1) Source: 1. Millero (1995).

Table B6
Formulation of essential biochemical processes (pelagic system).

Biochemical Processes	Formulation [min (a, b) = a (a < b), or b (a ≥ b); g(X, a_{half}) = X / (X + a_{half})]	Unit	Parameters [refer to Tables D]
[Phytoplankton (PP): 01]			
Biochemical net production / consumption	$\dot{C}_{pp} = Dpp_{pho} - Dpp_{ext} - Dpp_{res} - Dpp_{mor} - Dzp_{gra} - [Dpp_{sff}]_{(at\ sediment\text{-}water\ interface)}$	mgC/l/h	
Photosynthesis	$Dpp_{pho} = v_{pho01} \cdot u_{pho01a} \cdot u_{pho01b} \cdot PP$	mgC/l/h	
Maximum growth rate	$v_{pho01} = \alpha_{pho01} \cdot \exp(\beta_{pho01} \cdot TempW)$	1/h	α_{pho01}, β_{pho01}
Nutrient limitation	$u_{pho01a} = \min[g(WNX+WNY, Hf_{n,pho01}), g(WDP, Hf_{p,pho01})]$	-	$Hf_{n,pho01}$, $Hf_{p,pho01}$
Light availability	$u_{pho01b} = (I_0 e^{-kz} - I_{min01}) / ((I_0 e^{-kz} - I_{min01}) + (I_{hf01} - I_{min01})$	-	I_{hf01}, I_{min01}
Light attenuation	k: Calculated in model dependent on PP, ZP, WDE_i	1/cm	
Extra-release	$Dpp_{ext} = Dpp_{pho} \cdot 0.135 \cdot \exp(-0.00201 \cdot R_{chl} \cdot PP \cdot 10^3)$	mgC/l/h	R_{chl}
Respiration	$Dpp_{res} = \alpha_{res01} \cdot \exp(\beta_{res01} \cdot TempW) \cdot PP$	mgC/l/h	α_{res01}, β_{res01}
Mortality	$Dpp_{mor} = \alpha_{mor01} \cdot \exp(\beta_{mor01} \cdot TempW) \cdot PP$	mgC/l/h	α_{mor01}, β_{mor01}
Suspension feeders feeding (at sediment-water interface)	$Dpp_{sff} = \frac{PP}{PP+ZP+\sum_{i=1}^{3} WDE_i} \cdot \frac{1}{A_{Depq}} \cdot Dsfb_{fee}$	mgC/l/h	A_{Depq}
[Zooplankton (ZP): 02]			
Biochemical net production / consumption	$\dot{C}_{zp} = Dzp_{gra} - Dzp_{fec} - Dzp_{exc} - Dzp_{mor} - [Dzp_{sff}]_{(at\ sediment\text{-}water\ interface)}$	mgC/l/h	
Grazing	$Dzp_{gra} = \alpha_{gra02} \cdot \exp(\beta_{gra02} \cdot TempW) \cdot (1 - \exp(A_{ivl02} \cdot (A_{kai02} - PP))) \cdot ZP$	mgC/l/h	α_{gra02}, β_{gra02}, A_{ivl02}, A_{kai02}
Feces	$Dzp_{fec} = (1 - R_{ege02}) \cdot Dzp_{gra}$	mgC/l/h	R_{ege02}
Excretion	$Dzp_{exc} = (R_{ege02} - R_{grt02}) \cdot Dzp_{gra}$	mgC/l/h	R_{ege02}, R_{grt02}
Mortality	$Dzp_{mor} = \alpha_{mor02} \cdot \exp(\beta_{mor02} \cdot TempW) \cdot ZP$	mgC/l/h	α_{mor02}, β_{mor02}
Suspension feeders feeding (at sediment-water interface)	$Dzp_{sff} = \frac{ZP}{PP+ZP+\sum_{i=1}^{3} WDE_i} \cdot \frac{1}{A_{Depq}} \cdot Dsfb_{fee}$	mgC/l/h	A_{Depq}
[Detritus (WDE): 03, i] [i = 1 (fast-labile), 2 (slow-labile), 3 (refractory / very slow-labile)]			
Biochemical net production / consumption	$\dot{C}_{wde,i} = R_{pp,i} \cdot Dpp_{mor} + R_{pp,i} \cdot Dzp_{fec} + R_{zp,i} \cdot Dzp_{mor} - Dwde_{omi,i} - Dwde_{smi,i} - Dwde_{ami,i} - Dwde_{dec,i} + [-Dwde_{sff,i} + Dwde_{sfc,i}]_{(at\ sediment\text{-}water\ interface)}$	mgC/l/h	$R_{pp,i}$, $R_{zp,i}$ (i = 1,2,3)
Oxic mineralization	$Dwde_{omi,i} = m_{03,i} \cdot g(WDO, Hf_{o2w,omi}) \cdot WDE_i / G$	mgC/l/h	$Hf_{o2w,omi}$
Suboxic mineralization	$Dwde_{smi,i} = m_{03,i} \cdot g(WNY, Hf_{no3w,smi}) \cdot (1 - g(WDO, Hf_{o2w,smi})) \cdot WDE_i / G$	mgC/l/h	$Hf_{o2w,smi}$, $Hf_{no3w,smi}$
Anoxic mineralization	$Dwde_{ami,i} = m_{03,i} \cdot (1 - g(WNY, Hf_{no3w,ami})) \cdot (1 - g(WDO, Hf_{o2w,ami})) \cdot WDE_i / G$	mgC/l/h	$Hf_{o2w,ami}$, $Hf_{no3w,ami}$
Mineralization rate	$m_{03,i} = \alpha_{mi03,i} \cdot \exp(\beta_{mi03,i} \cdot TempW)$	1/h	$\alpha_{mi03,i}$, $\beta_{mi03,i}$ (i = 1,2,3)
	$G = g(WDO, Hf_{o2w,omi}) + g(WNY, Hf_{no3w,smi}) \cdot (1 - g(WDO, Hf_{o2w,smi})) + (1 - g(WNY, Hf_{no3w,ami})) \cdot (1 - g(WDO, Hf_{o2w,ami}))$	-	$Hf_{o2w,omi}$, $Hf_{o2w,smi}$, $Hf_{no3w,smi}$, $Hf_{o2w,ami}$, $Hf_{no3w,ami}$
Decomposition	$Dwde_{dec,i} = R_{dec03,i} \cdot (Dwde_{omi,i} + Dwde_{smi,i} + Dwde_{ami,i})$	mgC/l/h	$R_{dec03,i}$ (i = 1,2,3)
Suspension feeders feeding (at sediment-water interface)	$Dwde_{sff,i} = \frac{WDE_i}{PP+ZP+\sum_{i=1}^{3} WDE_i} \cdot \frac{1}{A_{Depq}} \cdot Dsfb_{fee}$	mgC/l/h	A_{Depq}
Suspension feeders feces (at sediment-water interface)	$Dwde_{sfc,i} = \frac{1}{\Delta z_{bot}} \cdot R_{ZWfec51} \cdot R_{FOD51,i} \cdot Dsfb_{fec}$ (Δz_{bot} is the thickness of bottom layer of the pelagic system)	mgC/l/h	$R_{ZWfec51}$, $R_{FOD51,i}$ (refer to table B4)
[Dissolved organic matter (WDM): 04, j] [j = 1 (labile), 2 (refractory)]			
Biochemical net production / consumption	$\dot{C}_{wdm,j} = R_{ext01,j} \cdot Dpp_{ext} + \sum_{i=1}^{3} R_{DOM,ji} \cdot Dwde_{dec,i} - Dwdm_{omi,j} - Dwdm_{smi,j} - Dwdm_{ami,j}$	mgC/l/h	$R_{ext01,j}$, $R_{DOM,ji}$ (i = 1,2,3, j = 1,2)
Oxic mineralization	$Dwdm_{omi,j} = m_{04,j} \cdot g(WDO, Hf_{o2w,omi}) \cdot WDM_j / G$	mgC/l/h	$Hf_{o2w,omi}$
Suboxic mineralization	$Dwdm_{smi,j} = m_{04,j} \cdot g(WNY, Hf_{no3w,smi}) \cdot (1 - g(WDO, Hf_{o2w,smi})) \cdot WDM_j / G$	mgC/l/h	$Hf_{o2w,smi}$, $Hf_{no3w,smi}$
Anoxic mineralization	$Dwdm_{ami,j} = m_{04,j} \cdot (1 - g(WNY, Hf_{no3w,ami})) \cdot (1 - g(WDO, Hf_{o2w,ami})) \cdot WDM_j / G$	mgC/l/h	$Hf_{o2w,ami}$, $Hf_{no3w,ami}$
Mineralization rate	$m_{04,j} = \alpha_{mi04,j} \cdot \exp(\beta_{mi04,j} \cdot TempW)$	1/h	$\alpha_{mi04,j}$, $\beta_{mi04,j}$ (j = 1,2)
[NH_4-N (WNX): 05]			
Biochemical net production / consumption	$\dot{C}_{wnx} = R_{nc01} \cdot Dpp_{res} + R_{nc01} \cdot Dzp_{exc} + Dwnx_{red} + \sum_{i=1}^{3} R_{nc03,i} \cdot (Dwde_{omi,i} + Dwde_{smi,i} + Dwde_{ami,i}) + \sum_{j=1}^{2} R_{nc04,j} \cdot (Dwdm_{omi,j} + Dwdm_{smi,j} + Dwdm_{ami,j}) - R_{nc01} \cdot Dpp_{pho} \cdot \frac{WNX}{WNX + WNY} - Dwnx_{nit} + \frac{1}{\Delta z_{bot}} \cdot [R_{ncFOD51} \cdot Dsfb_{exc}]_{(at\ sediment\text{-}water\ interface)}$ (Δz_{bot} is the thickness of bottom layer of the pelagic system)	mgN/l/h	R_{nc01}, $R_{nc03,i}$, $R_{nc04,j}$ (i = 1,2,3, j = 1,2), $R_{ncFOD51}$ (refer to Table B4)
Nitrification	$Dwnx_{nit} = \alpha_{nit05} \cdot \exp(\beta_{nit05} \cdot TempW) \cdot g(WDO, Hf_{o2,nit05}) \cdot WNX$	mgN/l/h	α_{nit05}, β_{nit05}, $Hf_{o2,nit05}$
Nitrate reduction	$Dwnx_{red} = (14/12) \cdot (4/(8 - 3 \cdot R_{den06})) \cdot (1 - R_{den06}) \cdot (\sum_{i=1}^{3} Dwde_{smi,i} + \sum_{j=1}^{2} Dwdm_{smi,j})$	mgN/l/h	R_{den06}

(*continued on next page*)

Table B6 (*continued*)

Biochemical Processes	Formulation [min (a, b) = a (a < b), or b (a ≥ b); g(X, a_{half}) = X / (X + a_{half})]	Unit	Parameters [refer to Tables D]
[NO_3-N(WNY): 06]			
Biochemical net production / consumption	$\dot{C}_{wny} = Dwnx_{nit} - Dwny_{den} - Dwnx_{red} - R_{nc01} \cdot Dpp_{pho} \cdot \frac{WNY}{WNX + WNY}$	**mgN/l/h**	R_{nc01}
De-nitrification	$Dwny_{den} = (14/12) \cdot (4/(8-3 \cdot R_{den06})) \cdot R_{den06} \cdot \left(\sum_{i=1}^{3} Dwde_{smi,i} + \sum_{j=1}^{2} Dwdm_{smi,j}\right)$	**mgN/l/h**	R_{den06}
[PO_4-P (WDP) : 07]			
Biochemical net production / consumption	$\dot{C}_{wdp} = R_{pc01} \cdot Dpp_{res} + R_{pc01} \cdot Dzp_{exc} + \sum_{i=1}^{3} R_{pc03,i} \cdot \left(Dwde_{omi,i} + Dwde_{smi,i} + Dwde_{ami,i}\right) + \sum_{j=1}^{2} R_{pc04,j} \cdot \left(Dwdm_{omi,j} + Dwdm_{smi,j} + Dwdm_{ami,j}\right) - R_{pc01} \cdot Dpp_{pho} + \frac{1}{\Delta z_{bot}} \cdot [R_{pcFOD51} \cdot Dsfb_{exc}]_{(at\ sediment\text{-}water\ interface)}$ (Δz_{bot} is the thickness of bottom layer of the pelagic system)	**mgP/l/h**	R_{pc01}, $R_{pc03,i}$, $R_{pc04,j}$ (i = 1,2,3, j = 1,2); $R_{pcFOD51}$ (refer to Table B4)
[ODU (WOU): 08]			
Biochemical net production / consumption	$\dot{C}_{wou} = (32/12) \cdot \left(\sum_{i=1}^{3} Dwde_{ami,i} + \sum_{j=1}^{2} Dwdm_{ami,j}\right) - Dwou_{aut} - Dwou_{oxi}$	**mg/l/h**	
Oxidation	$Dwou_{oxi} = \alpha_{oxi08} \cdot \exp(\beta_{oxi08} \cdot TempW) \cdot g(WDO, Hf_{o2,oxi08}) \cdot WOU + R_{oxi08} \cdot (32/12) \cdot \left(\sum_{i=1}^{3} Dwde_{ami,i} + \sum_{j=1}^{2} Dwdm_{ami,j}\right)$	**mg/l/h**	α_{oxi08}, β_{oxi08}, $Hf_{o2,oxi08}$, R_{oxi08}
Authigenic mineralization	$Dwou_{aut} = \alpha_{aut08} \cdot \exp(\beta_{aut08} \cdot TempW) \cdot WOU + R_{aut08a} \cdot Dwou_{oxi} + R_{aut08b} \cdot (32/12) \cdot \left(\sum_{i=1}^{3} Dwde_{ami,i} + \sum_{j=1}^{2} Dwdm_{ami,j}\right)$	**mg/l/h**	α_{aut08}, β_{aut08}, R_{aut08a}, A_{aut08b}
[Dissolved oxygen (WDO) : 09]			
Biochemical net production / consumption	$\dot{C}_{wdo} = \frac{32}{12} \cdot Dpp_{pho} - \frac{32}{12} \cdot Dpp_{res} - \frac{32}{12} \cdot Dzp_{exc} - \frac{32}{12} \cdot \left(\sum_{i=1}^{3} Dwde_{omi,i} + \sum_{j=1}^{2} Dwdm_{omi,j}\right) - 2 \cdot \frac{32}{14} \cdot Dwnx_{nit} - Dwou_{oxi} - \frac{1}{\Delta z_{bot}} \cdot \left[\frac{32}{12} \cdot (Dsfb_{exc} + Ddfb_{exc})\right]_{(at\ sediment\text{-}water\ interface)}$ (Δz_{bot} is the thickness of bottom layer of the pelagic system)	**mgO_2/l/h**	
[DIC (WTC): 10]			
Biochemical net production / consumption	$\dot{C}_{wtc} = - Dpp_{pho} + Dpp_{res} + Dzp_{res} + \sum_{i=1}^{3} \left(Dwde_{omi,i} + Dwde_{smi,i} + Dwde_{ami,i}\right) + \sum_{j=1}^{2} \left(Dwdm_{omi,j} + Dwdm_{smi,j} + Dwdm_{ami,j}\right) + Dwcc_{dis} + \frac{1}{\Delta z_{bot}} [\int_{z_{sed}} \sum_{i=1}^{3} \left(Ddet_{omi,i} + Ddet_{smi,i} + Ddet_{ami,i}\right) dz + \int_{z_{sed}} \sum_{j=1}^{2} \left(Ddom_{omi,j} + Ddom_{smi,j} + Ddom_{ami,j}\right) dz + Dsfb_{exc} - Dsfb_{she} + Ddfb_{exc} + Dbal_{res} + Dcac_{dis}]_{(at\ sediment\text{-}water\ interface)}$ (Δz_{bot} is the thickness of bottom layer of the pelagic system) (z_{sed} is the thickness of benthic system)	**mgC/l/h**	
$CaCO_3$ dissolution	$Dwcc_{dis} = (m_{dis10c} \cdot R_{ca10} + m_{dis10a} \cdot (1 - R_{ca10})) \cdot WCC$	**mgC/l/h**	R_{ca10}
Dissolution rate of calcite	$m_{dis10c} = R_{dis10c} \cdot \left(1.0 - \min\left(1.0, \frac{pCO_2 \cdot 1.0 \cdot 10^3}{1.025 \cdot 12.0 \cdot Cr_{10c}}\right)\right)$	l/h	R_{dis10c}
CO_3^{2-} Saturation concentration of calcite	$Cr_{10c} = 90.0 \cdot \exp\left(0.16 \cdot (z/10^5 - 4)\right)$	mmolC/gC	
Dissolution rate of aragonite	$m_{dis10a} = R_{dis10a} \cdot \left(1.0 - \min\left(1.0, \frac{pCO_2 \cdot 1.0 \cdot 10^3}{1.025 \cdot 12.0 \cdot Cr_{10a}}\right)\right)$	l/h	R_{dis10a}
CO_3^{2-} Saturation concentration of aragonite	$Cr_{10a} = 120.0 \cdot \exp\left(0.15 \cdot (z/10^5 - 4)\right)$ (Formulation of $CaCO_3$ dissolution is based on Broecker and Takahashi, 1978)	mmolC/gC	
SFB shell formation (at sediment-water interface)	$Dsfb_{she} = R_{sfb10} (Dsfb_{fec} - Dsfb_{fec} - Dsfb_{exc})$	**µgC/cm²/h**	R_{sfb10}

(*continued on next page*)

Table B6 (*continued*)

Biochemical Processes	Formulation [min (a, b) = a (a < b), or b (a ≥ b); g(X, a_{half}) = X / (X + a_{half})]	Unit	Parameters [refer to Tables D]
[$CaCO_3$ (WCC): 11] **Biochemical net production / consumption**	$\dot{C}_{wcc} = -Dwcc_{dis}$ (* refer to the bottom of Table B6)	**mgC/l/h**	
[Alkalinity (WAL): 12]			
Biochemical net production / consumption	$\dot{C}_{wal} = -Dwal_{pppho05} + Dwal_{pppho06} - Dwal_{ppres} - Dwal_{zpexc} + Dwal_{wnxnit} + Dwal_{wouoxi} + Dwal_{wccdiss} + \sum_{i=1}^{3}\left(R_{npc}^{03,omi,i}\cdot Dwde_{omi,i} + R_{npc}^{03,smi,i}\cdot Dwde_{smi,i} + R_{npc}^{03,ami,i}\cdot Dwde_{ami,i}\right) + \sum_{j=1}^{2}\left(R_{npc}^{04,omi,j}\cdot Dwdm_{omi,j} + R_{npc}^{04,smi,j}\cdot Dwdm_{smi,j} + R_{npc}^{04,ami,j}\cdot Dwdm_{ami,j}\right) + \frac{1}{\Delta z_{bot}}[-Dwal_{sfbexc} + Dwal_{sfbshe} - Dwal_{dfbexc} + \int_{z_{sed}}\sum_{i=1}^{3}\left(R_{npc}^{03,omi,i}\cdot Ddet_{omi,i} + R_{npc}^{03,smi,i}\cdot Ddet_{smi,i} + R_{npc}^{03,ami,i}\cdot Ddet_{ami,i}\right)dz + \int_{z_{sed}}\sum_{j=1}^{2}\left(R_{npc}^{04,omi,j}\cdot Ddom_{omi,j} + R_{npc}^{04,smi,j}\cdot Ddom_{smi,j} + R_{npc}^{04,ami,j}\cdot Ddom_{ami,j}\right)dz + \int_{z_{sed}}(Dwal_{hnxnit} + Dwal_{oduoxi})dz - Dwal_{balpho05} + Dwal_{balpho06} - Dwal_{balres} + Dwal_{cacdis}]_{(at\ sediment\text{-}water\ interface)}$ (Δz_{bot} is the thickness of bottom layer of the pelagic system) (z_{sed} is the thickness of benthic system)	**meq/l/h**	
	$R_{npc}^{03,omi,i} = \left(\frac{1}{14}R_{nc03,i} - \frac{1}{31}R_{pc03,i}\right)$ $R_{npc}^{03,smi,i} = \left(\frac{1}{14}R_{nc03,i} - \frac{1}{31}R_{pc03,i}\right) - 4\frac{2-x}{3x-8}$ $R_{npc}^{03,ami,i} = \left(\frac{1}{14}R_{nc03,i} - \frac{1}{31}R_{pc03,i}\right) + \frac{13}{3}$	-	$R_{nc03,i}$, $R_{pc03,i}$ (i = 1,2,3)
	$R_{npc}^{04,omi,j} = \left(\frac{1}{14}R_{nc04,j} - \frac{1}{31}R_{pc04,j}\right)$ $R_{npc}^{04,smi,j} = \left(\frac{1}{14}R_{nc04,j} - \frac{1}{31}R_{pc04,j}\right) - 4\frac{2-x}{3x-8}$ $R_{npc}^{04,ami,j} = \left(\frac{1}{14}R_{nc04,j} - \frac{1}{31}R_{pc04,j}\right) + \frac{13}{3}$ (refer to Table 1 for variable "x")	-	$R_{nc04,j}$, $R_{pc04,j}$ (j = 1,2)
PP Photosynthesis (using NH_4-N)	$Dwal_{pppho05} = R_{npc}^{01}\cdot Dpp_{pho}\cdot\frac{WNX}{WNX+WNY}$	**meq/l/h**	
PP Photosynthesis (using NO_3-N)	$Dwal_{pppho06} = R'^{01}_{npc}\cdot Dpp_{pho}\cdot\frac{WNY}{WNX+WNY}$	**meq/l/h**	
	$R_{npc}^{01} = \left(\frac{1}{14}R_{nc01} - \frac{1}{31}R_{pc01}\right)$, $R'^{01}_{npc} = \left(\frac{1}{14}R_{nc01} + \frac{1}{31}R_{pc01}\right)$	-	R_{nc01}, R_{pc01}
PP Respiration	$Dwal_{ppres} = R_{npc}^{01}\cdot Dpp_{res}$	**meq/l/h**	
ZP Excretion	$Dwal_{zpexc} = R_{npc}^{01}\cdot Dzp_{exc}$	**meq/l/h**	
NH_4-N nitrification	$Dwal_{wnxnit} = \frac{2}{14}\cdot Dwnx_{nit}$	**meq/l/h**	
ODU oxidation	$Dwal_{wouoxi} = \frac{13}{3}\cdot\frac{1}{32}\cdot Dwou_{oxi}$	**meq/l/h**	
$CaCO_3$ dissolution	$Dwal_{wccdis} = \frac{2}{12}\cdot Dwcc_{dis}$	**meq/l/h**	
SFB Excretion (at sediment-water interface)	$Dwal_{sfbexc} = R_{Zexc51}\cdot R_{npc}^{FOD51}\cdot Dsfb_{exc}$	**µeq/cm²/h**	R_{Zexc51} (refer to Table B4)
	$R_{npc}^{FOD51} = \left(\frac{1}{14}R_{ncFOD51} - \frac{1}{31}R_{pcFOD51}\right)$	-	$R_{ncFOD51}$, $R_{pcFOD51}$ (refer to Table B4)
SFB shell formation (at sediment-water interface)	$Dwal_{sfbshe} = \frac{2}{12}\cdot Dsfb_{she}$	**µeq/cm²/h**	
DFB Excretion (at sediment-water interface)	$Dwal_{dfbexc} = R_{Zexc52}\cdot R_{npc}^{FOD52}\cdot Ddfb_{exc}$	**µeq/cm²/h**	R_{Zexc52} (refer to Table B4)
	$R_{npc}^{FOD52} = \left(\frac{1}{14}R_{ncFOD52} - \frac{1}{31}R_{pcFOD52}\right)$	-	$R_{ncFOD52}$, $R_{pcFOD52}$ (refer to Table B4)
NH_4-N nitrification (at sediment-water interface)	$Dwal_{hnxnit} = \frac{2}{14}\cdot Dhnx_{nit}$	**meq/l/h**	
ODU oxidation (at sediment-water interface)	$Dwal_{oduoxi} = \frac{13}{3}\cdot\frac{1}{32}\cdot Dodu_{oxi}$	**meq/l/h**	
BAL photosynthesis (using NH_4-N) (at sediment-water interface)	$Dwal_{balpho05} = R_{npc}^{60}\cdot Dbal_{pho}\cdot\frac{R_{pho60,55}\cdot HNX}{R_{pho60,55}\cdot HNX+HNY}$	**µeq/cm²/h**	$R_{pho60,55}$
BAL photosynthesis (using NO_3-N) (at sediment-water interface)	$Dwal_{balpho06} = R'^{60}_{npc}\cdot Dbal_{pho}\cdot\frac{HNY}{R_{pho60,55}\cdot HNX+HNY}$	**µeq/cm²/h**	$R_{pho60,55}$
	$R_{npc}^{60} = \left(\frac{1}{14}R_{nc60} - \frac{1}{31}R_{pc60}\right)$, $R'^{60}_{npc} = \left(\frac{1}{14}R_{nc60} + \frac{1}{31}R_{pc60}\right)$	-	R_{nc60}, R_{pc60}
BAL Respiration (at sediment-water interface)	$Dwa_{balres} = R_{npc}^{60}\cdot Dbal_{res}$	**µeq/cm²/h**	
$CaCO_3$ dissolution (at sediment-water interface)	$Dwal_{cacdis} = \frac{2}{12}\cdot Dcac_{dis}$	**µeq/cm²/h**	

(*continued on next page*)

Table B6 (*continued*)

Biochemical Processes	Formulation [min (a, b) = a (a < b), or b (a ≥ b); g(X, a_{half}) = X / (X + a_{half})]	Unit	Parameters [refer to Tables D]
[pH (WPH): 13]			
Hydrogen ion concentration	$pH = -\log_{10} C_{H+}$ $C_{H+} = [H^+]$: hydrogen ion concentration **pH** is calculated from the equation representing the relationship between **TALK** and C_{H+} (refer to Dickson et al., 2007). The equation is solved for C_{H+} using a Newton-Raphson technique.	-	
[pCO_2 (WPS): 14]			
Gaseous carbon dioxide	$pCO_2 = \varphi_{pCO2} \cdot WTC$	µatm	
	$\frac{1}{\varphi_{pCO2}} = K_0\{1 + K_1/C_{H+} + K_1 \cdot K_2/(C_{H+})^2\}$	-	$K_0 = WCX/C_{H+}$ $K_1 = C_{H+} \cdot WCY/WCX$ $K_2 = C_{H+} \cdot WCZ/WCY$ (refer to Table B5)
[HCO_3^- (WCY): 15]			
Dissolved bicarbonate	$WCY = [HCO_3^-] = \frac{K_1 \cdot C_{H+} \cdot WTC}{(C_{H+})^2 + K_1 \cdot C_{H+} + K_1 \cdot K_2}$	mgC/l	
[CO_3^{2-} (WCZ): 16]			
Dissolved carbonate	$WCZ = [CO_3^{2-}] = K_2 \cdot WCY/C_{H+}$	mgC/l	
[CO_2* (WCX): 17]			
Dissolved carbonic acid	$WCX = [CO_2^*] = WTC - WCY - WCZ$	mgC/l	

*1) Shell formation of SFB was considered but that of plankton and deposit feeders in Fig. 3 was set at zero in this study.
*2) Formulation of $CaCO_3$ dissolution is based on Broecker and Takahashi, 1978.
*3) **pH** is calculated from the relationship between **TALK** and C_{H+} (refer to Dickson et al., 2007).

Table B7
Formulation of essential biochemical processes (benthic system).

Biochemical Processes	Formulation [min(a, b) = a (a < b), or b (a ≥ b); g(X,a_{half}) = X / (X + a_{half})]	Unit [`cm$^3$` represents volume of sum of solid and liquid phase]	Parameters [refer to Tables D]
[Suspension feeders (SFB): 51] (excluding hard shell ($CaCO_3$) fraction)			
Biochemical net production / consumption	$\dot{C}_{sfb} = Dsfb_{fee} - Dsfb_{fec} - Dsfb_{exc} - Dsfb_{mor} + Dsfb_{lar}$	**µgC/cm²/h**	
Feeding	$Dsfb_{fee} = min(Lim_{filter}, Lim_{growth})$	**µgC/cm²/h**	
Filter rate limitation	$Lim_{filter} = v_{fee51} \cdot u_{fee51} \cdot (PP + ZP + WDE_1 + WDE_2 + WDE_3) \cdot R_{cor0} \cdot SFB$	µgC/cm²/h	
Filter rate	$v_{fee51}=1.2\times10^{-5} \cdot tempB^{1.25} \cdot Aw_{wet51}{}^{-0.75}/A_{wd51}/A_{cd51}$ (tempB≥10) $1.2\times10^{-5} \cdot 10^{1.25} \cdot Aw_{wet51}{}^{-0.75}/A_{wd51}/A_{cd51}$ (tempB<10)	ml/h/µgC	Aw_{wet51}, A_{wd51}, A_{cd51}
Oxygen saturation limitation	$u_{fee51} = min(1, do_{sat}/R_{O2mor51})$ do_{sat}: Oxygen saturation of bottom water (calculated)	-	$R_{O2mor51}$
Decreasing by double filtering	$R_{cor0} = (1-exp(-COR0)) / COR0$	-	
Double filtering ratio	$COR0=v_{fee51} \cdot u_{fee51} \cdot SFB \cdot dt / A_{Depq}$	-	A_{Depq}
Growth rate limitation	$Lim_{growth} = (\alpha_{grt51}+\alpha_{bas51}) / (R_{ege51} \cdot (1- R_{exc51})) \cdot SFB \cdot F_{temp}$ F_{temp}: function of temperature	µgC/cm²/h	α_{grt51}, α_{bas51}, R_{ege51}, R_{exc51}
Feces	$Dsfb_{fec} = (1-R_{ege51}) \cdot Dsfb_{fee}$	**µgC/cm²/h**	R_{ege51}
Excretion	$Dsfb_{exc} = R_{exc51} \cdot R_{ege51} \cdot Dsfb_{fee} + \alpha_{bas51} \cdot SFB$	**µgC/cm²/h**	R_{exc51}, R_{ege51}, α_{bas51}
Mortality	$Dsfb_{mor} = v_{mor51} \cdot exp(\beta_{mor51} \cdot tempB) \cdot SFB$	**µgC/cm²/h**	β_{mor51}
Rate of mortality	$v_{mor51} = \alpha_{mor51a} + \alpha_{mor51b} \cdot (1-u_{fee51})$	1/h	α_{mor51a}, α_{mor51b}
Larva input	$Dsfb_{lar} = R_{lar51} \cdot Dsfb_{fee,av}$	**µgC/cm²/h**	R_{lar51}
	$Dsfb_{fee,av}$: spatial and temporal average of feeding(calculated)	µgC/cm²/h	
[Deposit feeders (DFB): 52]			
Biochemical net production / consumption	$\dot{C}_{dfb} = Ddfb_{fee} - Ddfb_{fec} - Ddfb_{exc} - Ddfb_{mor} + Ddfb_{lar}$	**µgC/cm²/h**	
Feeding	$Ddfb_{fee} = \alpha_{fee52} \cdot exp(\beta_{fee52} \cdot tempB) \cdot u_{fee52a} \cdot u_{fee52b} \cdot u_{fee52c} \cdot DFB$	**µgC/cm²/h**	α_{fee52}, β_{fee52}
Food limitation	$u_{fee52a} = 1-exp(A_{ivl52} \cdot min(0, A_{kai52}-Food_{52}))$ $Food_{52}$: average concentration of food in mud. (calculated)	-	A_{ivl52}, A_{kai52}
Cannibalism efficiency	$u_{fee52b} = g(DFB, Hf_{dfb,fee52})$	-	$Hf_{dfb,fee52}$
Oxygen saturation limitation	$u_{fee52c} = min(1, do_{sat} / R_{O2mor52})$	-	$R_{O2mor52}$
Feces	$Ddfb_{fec} = (1-u_{fee52}) \cdot Ddfb_{fee}$	**µgC/cm²/h**	
Assimilation efficiency	$u_{fec52} = 1-R_{undg52} \cdot (1 + g(Food_{52}, Hf_{fod52,fee52}))$	-	R_{undg52}, $Hf_{fod52,fee52}$
Excretion	$Ddfb_{exc} = R_{exc52} \cdot u_{fee52} \cdot Ddfb_{fee}$	**µgC/cm²/h**	R_{exc52}
Mortality	$Ddfb_{mor} = v_{mor52} \cdot u_{mor52} \cdot DFB$	**µgC/cm²/h**	
Rate of mortality	$v_{mor52} = \alpha_{mor52a} + \alpha_{mor52b} \cdot (1-u_{fee52c})$	1/h	α_{mor52a}, α_{mor52b}
Temperature dependency	$u_{mor52} = min(exp(\beta_{mor52} \cdot tempB), exp(\beta_{mor52} \cdot A_{temp,fee52}))$	-	$A_{temp,fee52}$, β_{mor52}
Larva input	$Ddfb_{lar} = R_{lar52} \cdot Ddfb_{fee,av}$	**µgC/cm²/h**	R_{lar52}
	$Ddfb_{fee,av}$: spatial and temporal average of feeding (calculated)	µgC/cm²/h	
[Detritus (DET): 53, i] [i = 1 (fast-labile), 2 (slow-labile), 3 (refractory/very slow-labile)]			
Biochemical net production / consumption	$\dot{C}_{det,i} = \frac{1}{\Delta z_{bl}} (R_{Zfec51} \cdot R_{FOD51,i} \cdot Dsfb_{fec} + R_{Zmor51} \cdot R_{SFB,i} \cdot Dsfb_{mor}$ $+ R_{Zfec52} \cdot R_{FOD52,i} \cdot Ddfb_{fec} + R_{Zmor52} \cdot R_{DFB,i} \cdot Ddfb_{mor}$ $- R_{Zfee52} \cdot R_{FOD52,i} \cdot Ddfb_{fee} + R_{Zmor60} \cdot R_{BAL,i} \cdot Dbal_{mor})$ $- Ddet_{omi,i} - Ddet_{smi,i} - Ddet_{ami,i} - Ddet_{dec,i}$ (Δz_{bl} is the thickness of any layer of the benthic system)	**µgC/cm³/h**	$R_{SFB,i}$, $R_{DFB,i}$, R_{BALi} (i = 1,2,3) R_{Zfec51}, R_{Zmor51}, R_{Zmor52} R_{Zfec52}, R_{zfee52}, R_{zmor60} (refer to table B4) $R_{FOD51,i}$, $R_{FOD52,i}$ (i =1,2,3) (refer to table B4)
Oxic mineralization	$Ddet_{omi,i} = m_{53,i} \cdot g(DOO, Hf_{o2b,omi}) \cdot DET_i / G \cdot (1-\varphi)$	**µgC/cm³/h**	$Hf_{o2b,omi}$
Suboxic mineralization	$Ddet_{smi,i} = m_{53,i} \cdot g(HNY, Hf_{no3b,smi}) \cdot (1-g(DOO, Hf_{o2b,smi})) \cdot DET_i / G \cdot (1-\varphi)$	**µgC/cm³/h**	$Hf_{o2b,smi}$, $Hf_{no3b,smi}$
Anoxic mineralization	$Ddet_{ami,i} = m_{53,i} \cdot (1-g(HNY, Hf_{no3b,ami})) \cdot (1-g(DOO, Hf_{o2b,ami})) \cdot DET_i / G \cdot (1-\varphi)$	**µgC/cm³/h**	$Hf_{o2b,ami}$, $Hf_{no3b,ami}$
Mineralization rate	$m_{53,i} = \alpha_{mi53,i} \cdot exp(\beta_{mi53,i} \cdot tempB)$	1/h	$\alpha_{mi53,i}$, $\beta_{mi53,i}$ (i=1,2,3)
	$G = g(DOO, Hf_{o2b,omi})$ $+ g(HNY, Hf_{no3b,smi}) \cdot (1-g(DOO, Hf_{o2b,smi}))$ $+ (1-g(HNY, Hf_{no3b,ami})) \cdot (1-g(DOO, Hf_{o2b,ami}))$	-	$Hf_{o2b,omi}$, $Hf_{o2b,smi}$, $Hf_{no3b,smi}$, $Hf_{o2b,ami}$, $Hf_{no3b,ami}$
Decomposition	$Ddet_{dec,i} = R_{dec53,i} \cdot (Ddet_{omi,i} + Ddet_{smi,i} + Ddet_{ami,i})$	**µgC/cm³/h**	$R_{dec53,i}$ (i = 1,2,3)
[Dissolved organic matter (DOM): 54, j] [j = 1 (labile), 2 (refractory)]			
Biochemical net production / consumption	$\dot{C}_{dom,j} = \frac{1}{\Delta z_{bl}} R_{ext60,j} \cdot Dbal_{ext} + \sum_{i=1}^{3} R_{DOM,ji} \cdot Ddet_{dec,i}$ $- \frac{1}{\Delta z_{bl}} R_{Zfee52} \cdot R_{FOD52,54j} \cdot Ddfb_{fee}$ $+ \frac{1}{\Delta z_{bl}} R_{Zfec52} \cdot R_{FOD52,54j} \cdot Ddfb_{fec}$ $- Ddom_{omi,j} - Ddom_{smi,j} - Ddom_{ami,j}$ (Δz_{bl} is the thickness of any layer of the benthic system)	**µgC/cm³/h**	$R_{ext60,j}$, $R_{DOM,ji}$ (i = 1,2,3, j = 1,2) R_{Zfec52}, R_{zfee52} (refer to table B4) $R_{FOD52,54j}$ (j =1,2) (refer to table B4)
Oxic mineralization	$Ddom_{omi,j} = m_{54,j} \cdot g(DOO, Hf_{o2b,omi}) \cdot DOM_j / G \cdot (\varphi + \overline{\rho}_s \cdot K_{ads54,j} \cdot (1-\varphi))$	**µgC/cm³/h**	$Hf_{o2b,omi}$, $K_{ads54,j}$ (j = 1,2)
Suboxic mineralization	$Ddom_{smi,j} = m_{54,j} \cdot g(HNY, Hf_{no3b,smi}) \cdot (1-g(DOO, Hf_{o2b,smi})) \cdot DOM_j / G \cdot (\varphi + \overline{\rho}_s \cdot K_{ads54,j} \cdot (1-\varphi))$	**µgC/cm³/h**	$Hf_{o2b,smi}$, $Hf_{no3b,smi}$, $K_{ads54,j}$ (j = 1,2)
Anoxic mineralization	$Ddom_{ami,j} = m_{54,j} \cdot (1-g(HNY, Hf_{no3b,ami})) \cdot (1-g(DOO, Hf_{o2b,ami})) \cdot DOM_j / G \cdot (\varphi + \overline{\rho}_s \cdot K_{ads54,j} \cdot (1-\varphi))$	**µgC/cm³/h**	$Hf_{o2b,ami}$, $Hf_{no3b,ami}$, $K_{ads54,j}$ (j = 1,2)
Mineralization rate	$m_{54,j} = \alpha_{mi54,j} \cdot exp(\beta_{mi54,j} \cdot TempB)$	1/h	$\alpha_{mi54,j}$, $\beta_{mi54,j}$ (j = 1,2)

(*continued on next page*)

Table B7 (*continued*)

Biochemical Processes	Formulation [min(a, b) = a (a < b), or b (a ≥ b); g(X, a_{half}) = X / (X + a_{half})]	Unit [‘cm^3’ represents volume of sum of solid and liquid phase]	Parameters [refer to Tables D]
[NH_4-N (HNX): 55]			
Biochemical net production / consumption	$\dot{C}_{hnx} = \frac{1}{\Delta z_{bl}}\cdot R_{nc60}\cdot Dbal_{res} + Dhnx_{red} + \sum_{i=1}^{3} R_{nc03,i}\cdot(Ddet_{omi,i}+Ddet_{smi,i}+Ddet_{ami,i}) + \sum_{j=1}^{2} R_{nc04,j}\cdot(Ddom_{omi,j}+Ddom_{smi,j}+Ddom_{ami,j}) - \frac{1}{\Delta z_{bl}}\cdot R_{nc60}\cdot Dbal_{pho}\cdot\frac{R_{pho60,55}\cdot HNX}{R_{pho60,55}\cdot HNX+HNY} - Dhnx_{nit} + \frac{1}{\Delta z_{bl}} R_{Zexc52}\cdot R_{ncFOD52}\cdot Ddfb_{exc}$ (Δz_{bl} is the thickness of any layer of the benthic system)	**µgN/cm³/h**	R_{nc60}, $R_{nc03,i}$, $R_{nc04,j}$, $R_{pho60,55}$ (i = 1,2,3, j = 1,2); R_{Zexc52}, $R_{ncFOD52}$ (refer to Table B4)
Nitrification	$Dhnx_{nit} = \alpha_{nit55}\cdot exp(\beta_{nit55}\cdot TempB)\cdot g(DOO,Hf_{o2,nit55})\cdot HNX\cdot(\varphi+\bar{\rho}_s\cdot K_{ads55}\cdot(1-\varphi))$	**µgN/cm³/h**	α_{nit55}, β_{nit55}, $Hf_{o2,\ nit55}$, K_{ads55}
Nitrate reduction	$Dhnx_{red} = (14/12)\cdot(4/(8-3\cdot R_{den56}))\cdot(1-R_{den56})\cdot(\sum_{i=1}^{3} Ddet_{smi,i} + \sum_{j=1}^{2} Ddom_{smi,j})$	**µgN/cm³/h**	R_{den56}
[NO_3-N (HNY): 56]			
Biochemical net production / consumption	$\dot{C}_{hny} = Dhnx_{nit} - Dhny_{den} - Dhnx_{red} - \frac{1}{\Delta z_{bl}}\cdot R_{nc60}\cdot Dbal_{pho}\cdot\frac{HNY}{R_{pho60,55}\cdot HNX+HNY}$ (Δz_{bl} is the thickness of any layer of the benthic system)	**µgN/cm³/h**	R_{nc60}, $R_{pho60,\ 55}$
De-nitrification	$Dhny_{den} = (14/12)\cdot(4/(8-3\cdot R_{den56}))\cdot R_{den56}\cdot(\sum_{i=1}^{3} Ddet_{smi,i} + \sum_{j=1}^{2} Ddom_{smi,j})$	**µgN/cm³/h**	R_{den56}
[PO_4-P (DIP): 57]			
Biochemical net production / consumption	$\dot{C}_{dip} = \frac{1}{\Delta z_{bl}}\cdot R_{pc60}\cdot Dbal_{res} + \sum_{i=1}^{3} R_{pc03,i}\cdot(Ddet_{omi,i}+Ddet_{smi,i}+Ddet_{ami,i}) + \sum_{j=1}^{2} R_{pc04,j}\cdot(Ddom_{omi,j}+Ddom_{smi,j}+Ddom_{ami,j}) - \frac{1}{\Delta z_{bl}}\cdot R_{pc60}\cdot Dbal_{pho} + \frac{1}{\Delta z_{bl}}\cdot R_{Zexc52}\cdot R_{pcFOD52}\cdot Ddfb_{exc}$ (Δz_{bl} is the thickness of any layer of the benthic system)	**µgP/cm³/h**	R_{pc60}, $R_{pc03,i}$, $R_{pc04,j}$ (i = 1,2,3, j = 1,2); R_{Zexc52}, $R_{pcFOD52}$ (refer to Table B4)
[ODU (ODU): 58]			
Biochemical net production / consumption	$\dot{C}_{odu} = (32/12)\cdot(\sum_{i=1}^{3} Ddet_{ami,i} + \sum_{j=1}^{2} Ddom_{ami,j}) - Dodu_{aut} - Dodu_{oxi}$	**µg/cm³/h**	
Oxidation	$Dodu_{oxi} = \alpha_{oxi58}\cdot exp(\beta_{oxi58}\cdot tempB)\cdot g(DOO, Hf_{o2,oxi58})\cdot ODU\cdot\varphi + R_{oxi58}\cdot(32/12)\cdot(\sum_{i=1}^{3} Ddet_{ami,i} + \sum_{j=1}^{2} Ddom_{ami,j})$	**µg/cm³/h**	α_{oxi58}, β_{oxi58}, $Hf_{o2,oxi58}$, R_{oxi58}
Authigenic mineralization	$Dodu_{aut} = \alpha_{aut58}\cdot exp(\beta_{aut58}\cdot tempB)\cdot ODU\cdot\varphi + R_{aut58a}\cdot Dodu_{oxi} + R_{aut58b}\cdot(32/12)\cdot(\sum_{i=1}^{3} Ddet_{ami,i} + \sum_{j=1}^{2} Ddom_{ami,j})$	**µg/cm³/h**	α_{aut58}, β_{aut58}, R_{aut58a}, R_{aut58b}
[Dissolved oxygen (DOO): 59]			
Biochemical net production / consumption	$\dot{C}_{doo} = \frac{1}{\Delta z_{bl}}\cdot R_{Zpho60}\cdot\frac{32}{12}\cdot Dbal_{pho} - \frac{1}{\Delta z_{bl}}\cdot R_{Zres60}\cdot\frac{32}{12}\cdot Dbal_{res} - \frac{32}{12}\cdot(\sum_{i=1}^{3} Ddet_{omi,i} + \sum_{j=1}^{2} Ddom_{omi,j}) - 2\cdot\frac{32}{14}\cdot Dhnx_{nit} - Dodu_{oxi}$ (Δz_{bl} is the thickness of any layer of the benthic system)	**µg/cm³/h**	R_{Zpho60}, R_{Zres60} (refer to Table B4)
[Benthic algae (BAL): 60]			
Biochemical net production / consumption	$\dot{C}_{bal} = Dbal_{pho} - Dbal_{ext} - Dbal_{res} - Dbal_{mor} - R_{FOD52,60}\cdot Ddfb_{fee}$	**µgC/cm²/h**	$R_{FOD52,60}$ (refer to Table B4)
Photosynthesis	$Dbal_{pho} = v_{pho60}\cdot u_{pho60a}\cdot u_{pho60b}\cdot BAL\cdot R_{Zpho60}$	**µgC/cm²/h**	R_{Zpho60} (refer to Table B4)
Maximum growth rate	$v_{pho60} = \alpha_{pho60}\cdot exp(\beta_{pho60}\cdot TempB)$	1/h	α_{pho60}, β_{pho60}
Nutrient limitation	$u_{pho60a} = \min[\ g(HNX+HNY, Hf_{n,pho60}), g(DIP, Hf_{p,pho60})\ ]$	-	$Hf_{n,\ pho60}$, $Hf_{p,\ pho60}$
Light availability	$u_{pho60b} = \frac{1}{\Delta z_p}\int_z^{z+\Delta z_p}\frac{I_B}{I_{opt60}}e^{-k_b z}\cdot exp\left(1-\frac{I_B}{I_{opt60}}e^{-k_b z}\right)dz$	-	I_{opt60}, k_b
Extra-release	$Dbal_{ext} = R_{ext60}\cdot Dbal_{pho}$	**µgC/cm²/h**	R_{ext60}
Respiration	$Dbal_{res} = R_{res60a}\cdot exp(\beta_{pho60}\cdot TempB)\cdot g(DOO, Hf_{o2,res60})\cdot BAL\cdot R_{Zres60} - R_{res60b}\cdot Dbal_{pho}$	**µgC/cm²/h**	R_{res60a}, β_{pho60}, $Hf_{o2,\ res60}$, R_{res60b}, R_{Zres60} (refer to Table B4)
Mortality	$Dbal_{mor} = v_{mor60}\cdot BAL\cdot R_{Zmor60}$	**µgC/ cm²/h**	R_{Zmor60} (refer to Table B4)
Rate of mortality	$v_{mor60} = \alpha_{mor60}\cdot exp(\beta_{mor60}\cdot TempB)$ (Δz_p is the thickness of photic benthic layer)	1/h	α_{mor60}, β_{mor60}
[$CaCO_3$(CAC): 63]			
Biochemical net production / consumption	$\dot{C}_{cac} = Dsfb_{she} - Dcac_{dis}$	**µgC/cm²/h**	
$CaCO_3$ dissolution	$Dcac_{dis} = (m_{dis63c}\cdot R_{ca63} + m_{dis63a}\cdot(1-R_{ca63}))\cdot(1-\varphi_{av})\cdot CAC$ (φ_{av} is vertical average of porosity φ)	**µgC/cm²/h**	$R_{ca63}=R_{ca10}$ (refer to Tables B6 and D3)
Dissolution rate of calcite	$m_{dis63c} = R_{dis63c}\cdot\left(1.0-\min\left(1.0, \frac{pCO_2\cdot 1.0\cdot 10^3}{1.025\cdot 12.0\cdot Cr_{63c}}\right)\right)$	**1/h**	$R_{dis63c}=R_{dis10c}$ (refer to Tables B6 and D3)
CO_3^{2-} Saturation concentration of calcite	$Cr_{63c} = 90.0\cdot exp\left(0.16\cdot(z/10^5 - 4)\right)$	**mmolC/gC**	
Dissolution rate of aragonite	$m_{dis63a} = R_{dis63a}\cdot\left(1.0 - \min\left(1.0, \frac{pCO_2\cdot 1.0\cdot 10^3}{1.025\cdot 12.0\cdot Cr_{63a}}\right)\right)$	**1/h**	$R_{dis63a}=R_{dis10a}$ (refer to Tables B6 and D3)
CO_3^{2-} Saturation concentration of aragonite	$Cr_{63a} = 120.0\cdot exp\left(0.15\cdot(z/10^5 - 4)\right)$ (Formulation of $CaCO_3$ dissolution is based on Broecker and Takahashi, 1978)	**mmolC/gC**	
Shell formation of SFB	$Dsfb_{she}$ (Refer to Table B6)	**µgC/cm²/h**	

*1) Model variables of DIC and total alkalinity in the benthic system are omitted and the production/consumption of DIC and total alkalinity in the benthic system are counted at the bottom layer in the pelagic system.

*2) Shell formation of SFB was considered but that of plankton and deposit feeders in Fig. 3 was set at zero in this study.

Appendix C. Formulations of air-sea CO_2 gas exchange

The air-sea CO_2 gas exchange is described as being proportional to the differences between pCO_2 in the air and the sea surface:

$$F_{CO_2}^{net} = \int_S F_{CO_2} ds = \int_S E\,(PCO_{2,\mathrm{air}} - PCO_{2,\mathrm{sea}})\,ds \tag{C1}$$

where $F_{CO_2}^{net}$ is the net-flux of CO_2 between the air and sea systems, $pCO_{2,air}$ is the partial pressure of CO_2 in the air, and $pCO_{2,sea}$ is the partial pressure of CO_2 at the sea surface. The proportionality variable E is the CO_2 exchange coefficient and is expressed as a function of seasonal variation (Table C1).

Table C1
Values of parameters related to the exchange of CO_2 across the air-sea interface.

Name	Unit	Value	Description	Major Source *1)
[air-sea CO_2 gas exchange]				
E	$mol{\cdot}m^{-2}{\cdot}y^{-1}{\cdot}\mu atm^{-1}$	0.064	CO_2 exchange coefficient (annual average value is indicated here)	1

*1) Source: 1. Sorai and Ohsumi (2005).

Appendix D. Values of biochemical parameters

The values of biochemical parameters are listed in Tables D1–D3. First, the parameters, either analyzed or calculated based on observations in Tokyo Bay, were set within the known ranges in the region of consideration (indicated as "OD" at item "Source" in Tables D1–D3). Next, the parameters whose values were estimated from the data in other coastal areas were set and indicated as "OE" at item "Source." Finally, the values of unknown parameters were set to fine-tune the simulation.

Table D1
Values of major biochemical parameters in the pelagic system (refer to Tables B).

Name	Unit	Value	Description	Major Source *1)
[Phytoplankton : 01]				
α_{pho01}, β_{pho01}	1/h, 1/℃	0.0625, 0.0693	Maximum growth rate	1,2, Q_{10} = 2
$Hf_{n,pho01}$	mgN/l	0.1	Half saturation constant for nitrogen limitation	3
$Hf_{p,pho01}$	mgP/l	0.05	Half saturation constant for phosphorus limitation	4
I_{min01}	$\mu E/m^2/s$	7.1	Minimum light intensity for photosynthesis	5
I_{hf01}	$\mu E/m^2/s$	56.5	Half saturation constant for light	5
R_{chl}	gChl-a/gC	0.0333	Chl-a:C ratio	6
α_{res01}, β_{res01}	1/h, 1/℃	0.00125, 0.0693	Rate of respiration	7, Q_{10} = 2
α_{mor01}, β_{mor01}	1/h, 1/℃	0.00042, 0.0693	Rate of mortality	Tu, Q_{10} = 2
R_{nc01}	gN/gC	0.2094	Ratio of nitrogen to carbon	8
R_{pc01}	gP/gC	0.0338	Ratio of phosphate to carbon	8
$R_{PP,1}$, $R_{PP,2}$, $R_{PP,3}$	–	0.85, 0.10, 0.05	Composition ratio (ratio of fast-labile, slow-labile and refractory / very slow-labile part)	Tu
$R_{ext01,1}$, $R_{ext01,2}$	–	0.2, 0.8	Ratio of labile and refractory DOM to extra-release	Tu
[Zooplankton : 02]				
α_{gra02}, β_{gra02}	1/h, 1/℃	0.0150, 0.0693	Maximum ratio	9, Q_{10} = 2
A_{ivl02}	l/mgC	6.3	Ivlev's constant	10, 11
A_{kai02}	$\mu gC/cm^3$	0.1	Feeding threshold	Tu
R_{ege02}	–	0.7	Assimilation efficiency	12, 13
R_{grt02}	–	0.3	Growth efficiency	11
α_{mor02}, β_{mor02}	1/h	0.0021, 0.0693	Rate of mortality	Tu
$R_{ZP,1}$, $R_{ZP,2}$, $R_{ZP,3}$	–	0.80, 0.15, 0.05	Composition ratio (ratio of fast-labile, slow-labile and refractory/very slow-labile part)	Tu
[Detritus, Dissolved organic matter : 03, i(i = 1,2,3), 04, j(j = 1,2)]				
$\alpha_{mi03,1}$, $\beta_{mi03,1}$	1/h, 1/℃	5.0×10^{-4}, 0.0693	Mineralization rate of fast-labile detritus	14,15,16,17,
$\alpha_{mi03,2}$, $\beta_{mi03,2}$	1/h, 1/℃	5.0×10^{-5}, 0.0693	Mineralization rate of slow-labile detritus	Q_{10} = 2
$\alpha_{mi03,3}$, $\beta_{mi03,3}$	1/h, 1/℃	5.0×10^{-7}, 0.0693	Mineralization rate of refractory/very slow-labile detritus	
$\alpha_{mi04,1}$, $\beta_{mi04,1}$	1/h, 1/℃	1.0×10^{-3}, 0.0693	Mineralization rate of fast-labile DOM	17, 18,
$\alpha_{mi04,2}$, $\beta_{mi04,2}$	1/h, 1/℃	0.0, 0.0693	Mineralization rate of refractory DOM	Q_{10} = 2
$Hf_{o2w,omi}$	mgO_2/l	0.096	Half saturation constant for O_2 limitation in oxic mineralization	19
$Hf_{o2w,smi}$	mgO_2/l	0.32	Half saturation constant for O_2 inhibition in suboxic mineralization	19
$Hf_{no3w,smi}$	mgN/l	1.86	Half saturation constant for NO_3 limitation in suboxic mineralization	19(OE)
$Hf_{o2w,ami}$	mgO_2/l	0.16	Half saturation constant for O_2 inhibition in anoxic mineralization	19
$Hf_{no3w,ami}$	mgN/l	0.50	Half saturation constant for NO_3 inhibition in anoxic mineralization	19(OE)
$R_{dec03,1}$	–	0.25	Ratio of decomposition to mineralization (fast-labile detritus)	15
$R_{dec03,2}$	–	0.25	Ratio of decomposition to mineralization (slow-labile detritus)	15
$R_{dec03,3}$	–	0.25	Ratio of decomposition to mineralization (refractory/very slow-labile detritus)	15
$R_{nc03,1}$	gN/gC	0.2235	Ratio of nitrogen to carbon (fast-labile detritus)	20(OD),8(OE)
$R_{nc03,2}$	gN/gC	0.1570	Ratio of nitrogen to carbon (slow-labile detritus)	
$R_{nc03,3}$	gN/gC	0.0739	Ratio of nitrogen to carbon (refractory/very slow-labile detritus)	
$R_{nc04,1}$	gN/gC	0.2401	Ratio of nitrogen to carbon (labile DOM)	
$R_{nc04,2}$	gN/gC	0.0739	Ratio of nitrogen to carbon (refractory DOM)	

(*continued on next page*)

Table D1 (*continued*)

Name	Unit	Value	Description	Major Source *1)
$R_{pc03,1}$	gP/gC	0.0362	Ratio of phosphate to carbon (fast-labile detritus)	20(OD),8(OE)
$R_{pc03,2}$	gP/gC	0.0210	Ratio of phosphate to carbon (slow-labile detritus)	
$R_{pc03,3}$	gP/gC	0.0020	Ratio of phosphate to carbon (refractory/very slow-labile detritus)	
$R_{pc04,1}$	gP/gC	0.0400	Ratio of phosphate to carbon (labile DOM)	
$R_{pc04,2}$	gP/gC	0.0020	Ratio of phosphate to carbon (refractory DOM)	
$R_{DOM,11}$, $R_{DOM,21}$	–	0.9, 0.1	Ratio of labile and refractory DOM to decomposition (fast-labile detritus)	Tu
$R_{DOM,12}$, $R_{DOM,22}$	–	0.5, 0.5	Ratio of labile and refractory DOM to decomposition (slow-labile detritus)	Tu
$R_{DOM,13}$, $R_{DOM,23}$	–	0.0, 1.0	Ratio of labile and refractory DOM to decomposition (refractory /very slow-labile detritus)	Tu
[NH_4-N, NO_3-N : 05, 06]				
α_{nit05}, β_{nit05}	1/h, 1/℃	0.001, 0.0693	Rate of nitrification	21 (OE),Q_{10} = 2
$Hf_{o2,nit05}$	mgO_2/l	0.032	Half saturation constant for O_2 limitation in nitrification	22(OE)
R_{den06}	–	0.75	Denitrification ratio to suboxic mineralization	Tu
[ODU : 08]				
α_{oxi08}, β_{oxi08}	1/h, 1/℃	1.0, 0.0693	Rate of ODU oxidation	19(OE),Q_{10} = 2
$Hf_{o2,oxi08}$	mgO_2/l	0.032	Half saturation constant for O_2 limitation in ODU oxidation	19
R_{oxi08}	–	0.0	Ratio of ODU oxidation to anoxic mineralization	Tu
α_{aut08}, β_{aut08}	1/h, 1/℃	0.0, 0.0	Rate of authigenic mineralization	Tu
R_{aut08a}	–	0.0	Ratio of authigenic mineralization to ODU oxidation	Tu
R_{aut08b}	–	0.0	Ratio of authigenic mineralization to ODU production	Tu

*1) Source : 1. Macedo et al. (2001); 2. Horiguchi (2001); 3. Epply et al.(1969); 4. Fuhs et al.(1972); 5. Nishikawa et al. (2002); 6.Strickland (1965); 7. Jørgensen et al. (1991); 8. Jørgensen (1979); 9. Baretta and Ruardij (1988); 10. Zillioux (1970); 11. Suschenya (1970); 12. Marshall and Orr (1955a); 13. Marshall and Orr (1955b); 14. Matsunaga (1981); 15. Ishikawa and Nishimura (1983); 16. Ogura (1972); 17. Emerson and Hedges (1988); 18. Ogura (1975); 19. Soetaert et al. (1996); 20. National Institute for Land and Infrastructure Management, 2006; 21. Jørgensen and Bendoricchio (2001); 22. Oguz (2002) Tu. Tuning. (OD: Observed data in Tokyo Bay; OE. Order estimated value referred to the literature.).

*2) Some of the values from these sources were not used directly but were used after analysis to convert the format of the model parameters.

Table D2
Values of major biochemical parameters in the benthic system (refer to Tables B).

Name	Unit	Value	Description	Major Source *1)
[Suspension feeders : 51]				
Aw_{wet51}	gw/ind	0.436	Basal weight	1, 2 (OD), 3
Aw_{d51}	gd/gw	0.05	Dry weight : wet weight ratio	1(OD)
A_{cd51}	gC/gd	0.328	Carbon : dry weight ratio	3
A_{Depq}	cm	100	Double filtering effective depth	Tu
$R_{O2mor51}$	–	0.15	Oxygen saturation occurring suspension feeder's mortality from oxygen deficiency	4,5 (OE)
α_{grt51}	1/h	0.002208	Efficient growth rate	6
α_{bas51}	1/h	0.0001256	Basal metabolism	7
R_{ege51}	–	0.6	Digestivity efficiency	8,9
R_{exc51}	–	0.9	Activity metabolism	7
β_{mor51}	1/℃	0.0693	Temperature dependency of mortality	Q_{10} = 2
α_{mor51a}	1/h	0.00017	Natural mortality rate at 0 ℃	Tu
α_{mor51b}	1/h	0.017	Rate of mortality from oxygen deficiency	Tu
R_{lar51}	–	0.01	Ratio of larva input to feeding	10
$R_{SFB,1}$, $R_{SFB,2}$, $R_{SFB,3}$	–	0.98, 0.01, 0.01	Composition ratio (ratio of fast-labile, slow-labile and refractory/very slow-labile part)	Tu
$R_{ZWfec51}$	–	0.5	Ratio of feces to pelagic system	Tu
[Deposit feeders : 52]				
α_{fee52}, β_{fee52}	1/h, 1/℃	0.0058, 0.0693	Maximum ratio	11(OE),Q_{10} = 2
$A_{temp,fee52}$	℃	10	Maximum saturation temperature about eating	12
A_{ivl52}	cm^3/μgC	0.005	Ivlev's constant	Tu
A_{kai52}	μgC/cm^3	200	Feeding threshold	7(OE)
$Hf_{dfb,fee52}$	μgC/cm^2	150	Half saturation constant for cannibalism efficiency	7(OE)
$R_{O2mor52}$	–	0.1	DO saturation occurring deposit feeders' mortality from oxygen deficiency	Tu
$Hf_{fod52,fee52}$	μgC/cm^2	2500.0	Half saturation constant for digestive efficiency	7(OE)
R_{undg52}	–	0.4	Minimum undigestive efficiency	13
R_{exc52}	–	0.61	Ratio of excretion to assimilated food	7(OE)
β_{mor52}	1/℃	0.0693	Temperature dependency of mortality	Q_{10} = 2
α_{mor52a}	1/h	0.00025	Natural mortality rate at 0 ℃	Tu
α_{mor52b}	1/h	0.0025	Rate of mortality from oxygen deficiency	Tu
R_{lar52}	–	0.01	Ratio of larva input to feeding	10
$R_{DFB,1}$, $R_{DFB,2}$, $R_{DFB,3}$	–	0.55, 0.40, 0.05	Composition ratio (ratio of fast-labile, slow-labile and refractory/very slow-labile part)	Tu
[Detritus, Dissolved organic matter : 53, i(i = 1,2,3), 54, j(j = 1,2)]				
$Hf_{o2b,omi}$	mgO_2/l	0.001	Half saturation constant for O_2 limitation in oxic mineralization	Tu
$Hf_{o2b,smi}$	mgO_2/l	1.00	Half saturation constant for O_2 inhibition in suboxic mineralization	14(OE)
$Hf_{o2b,ami}$	mgO_2/l	0.03	Half saturation constant for O_2 inhibition in anoxic mineralization	Tu
$Hf_{no3b,smi}$	mgN/l	0.16	Half saturation constant for NO_3 limitation in suboxic mineralization at oxic layer	14(OE)
$Hf_{no3b,ami}$	mgN/l	0.32	Half saturation constant for NO_3 inhibition in anoxic mineralization at oxic layer	14(OE)
$\alpha_{mi53,1}$, $\beta_{mi53,1}$	1/h, 1/℃	5.0×10^{-4}, 0.0693	Maximum mineralizatoin rate of fast labile detritus	15,16,17,18, Q_{10} = 2
$\alpha_{mi53,2}$, $\beta_{mi53,2}$	1/h, 1/℃	5.0×10^{-5}, 0.0693	Maximum mineralization rate of slow labile detritus	
$\alpha_{mi53,3}$, $\beta_{mi53,3}$	1/h, 1/℃	5.0×10^{-7}, 0.0693	Maximum mineralization rate of refractory/very slow labile detritus	

(*continued on next page*)

Table D2 (*continued*)

Name	Unit	Value	Description	Major Source *1)
$\alpha_{mi54,1}$, $\beta_{mi54,1}$	1/h, 1/℃	1.0×10^{-3}, 0.0693	Maximum mineralization rate of labile DOM	18, 19, Q_{10} = 2
$\alpha_{mi54,2}$, $\beta_{mi54,2}$	1/h, 1/℃	0, 0.0693	Maximum mineralization rate of refractory DOM	
$R_{dec53,1}$	–	0.1	Ratio decomposition to mineralization (fast-labile detritus)	Tu
$R_{dec53,2}$	–	0.25	Ratio decomposition to mineralization (slow-labile detritus)	20
$R_{dec53,3}$	–	0.25	Ratio decomposition to mineralization (refractory/very slow-labile detritus)	20
$K_{ads54,1}$, $K_{ads54,2}$	ml/g	25.03, 0.69	Adsorption coefficient for labile DOM and refractory DOM	Tu
[NH_4-N, NO_3-N : 55,56]				
α_{nit55}, β_{nit55}	1/h, 1/℃	0.3, 0.0693	Rate of nitrification	14(OE), Q_{10} = 2
$Hf_{o2,nit55}$	mgO_2/l	0.032	Half saturation constant for O_2 limitation in nitrification	14
R_{den56}	–	0.75	Denitrification ratio to suboxic mineralization	Tu
K_{ads55}	ml/g	1.58	Adsorption coefficient	21
[ODU : 58]				
α_{oxi58}, β_{oxi58}	1/h, 1/℃	5, 0.0693	Rate of oxidation	14(OE),Q_{10} = 2
$Hf_{o2,oxi58}$	mgO_2/l	0.032	Half saturation constant for O_2 limitation in oxidation	14
R_{oxi58}	–	0.0	Ratio of ODU oxidation to anoxic mineralization	Tu
α_{aut58}, β_{aut58}	1/h, 1/℃	0.0, 0.0	Rate of authigenic mineralization	Tu
R_{aut58a}	–	0.0	Ratio of authigenic mineralization to ODU oxidation	Tu
R_{aut58b}	–	0.0	Ratio of authigenic mineralization to ODU production	Tu
[Benthic algae : 60]				
α_{pho60}, β_{pho60}	1/h, 1/℃	0.045, 0.0693	Maximum growth rate	7, 22(OE), Q_{10} = 2
$Hf_{n,pho60}$	mgN/l	0.018	Half saturation constant for nitrogen limitation	23
$Hf_{p,pho60}$	mgP/l	0.001	Half saturation constant for phosphorus limitation	24
$Hf_{o2,res60}$	mg/l	0.03	Half saturation constant for oxygen limitation to respiration	Tu
I_{opt60}	μE/m^2/sec	30	Half saturation constant for light limitation	25
k_b	1/cm	59.0	Light attenuation coefficient in sediment	26(OE)
$R_{pho60,55}$	–	10	Ammonium intake ratio coefficient	Tu
R_{ext60}	–	0.122	Ratio of extra-release to photosynthesis	Tu
R_{res60a}	–	0.0002	Ratio of rest respiration rate to maximum growth rate	7
R_{res60b}	–	0.1	Ratio of activity respiration to photosynthesis	7(OE)
α_{mor60}, β_{mor60}	1/h, 1/℃	0.00019, 0.0693	Rate of natural mortality	7
R_{nc60}	gN/gC	0.2148	Ratio of nitrogen to carbon	24
R_{pc60}	gP/gC	0.0342	Ratio of phosphate to carbon	24
$R_{BAL,1}$, $R_{BAL,2}$, $R_{BAL,3}$	–	0.900, 0.075, 0.025	Composition ratio (ratio of fast-labile, slow-labile and refractory/very slow-labile part)	Tu
$R_{ext60,1}$, $R_{ext60,2}$	–	0.1, 0.9	Ratio of labile and refractory DOM to extra-release	Tu

*1) Source : 1. Kuwae(2001); 2. Kuwae et al.(2005); 3. Japan Environmental Management Association for Industry (1998); 4. Kurashige(1942); 5. Kakino (1982); 6. Isono et al.(1998); 7. Barreta and Ruardij (1988); 8. Yamamuro and Koike (1993); 9. Hiwatari et al. (2002); 10.Conover (1978); 11. Cammen (1980); 12.Kremer and Nixon (1978), 13. Valiela (1984); 14. Soetaert et al. (1996); 15. Matsunaga (1981); 16. Ishikawa and Nishimura (1983); 17. Ogura (1972); 18. Emerson and Hedges (1988); 19. Ogura (1975); 20. Ishikawa et al. (1983); 21. Rosenfeld (1979) 22. Admiraal et al. (1982); 23. Epply et al. (1969); 24. Jørgensen (1979); 25. Hiroshima Environment and Health Association (2002);26. Kamio et al. (2004); Tu. Tuning. (OD: Observed data in Tokyo Bay; OE: Order estimated value referred to the literature).

*2) Some of the values from these sources were not used directly but were used after analysis to convert the format of the model parameters.

Table D3
Values of major biochemical parameters in the carbon dioxicide system (refer to Tables B).

Name	Unit	Value	Description	Major Source *1)
[DIC (WTC):10]				
R_{dis10c}	1/h	0.048	Calcite dissolution rate	Tu
R_{dis10a}	1/h	0.144	Aragonite dissolution rate	Tu
R_{ca10}	–	0.7	Ratio of calcite to $CaCO_3$	Tu
R_{sfb10}	–	1.7	Ratio of $CaCO_3$ to organic cell (Suspension feeders)	Tu

*1) Tu. Tuning.

Appendix E. Reproducibility of model outputs for the carbon-nutrients-oxygen cycling system and food-web system

The sample of the model outputs and the observed data related to the seasonal variations in phytoplankton, detritus, DOC, nutrients, deposit feeders, suspension feeders, and dissolved oxygen in the pelagic and benthic systems are shown in Figs. E1 and E2. The reproducibility of model outputs related to the carbon-nutrients-oxygen cycling system and food-web system (Figs. E1 and E2) is almost identical to that given in Sohma et al. (2008), even though the carbonate chemistry system is incorporated in the model.

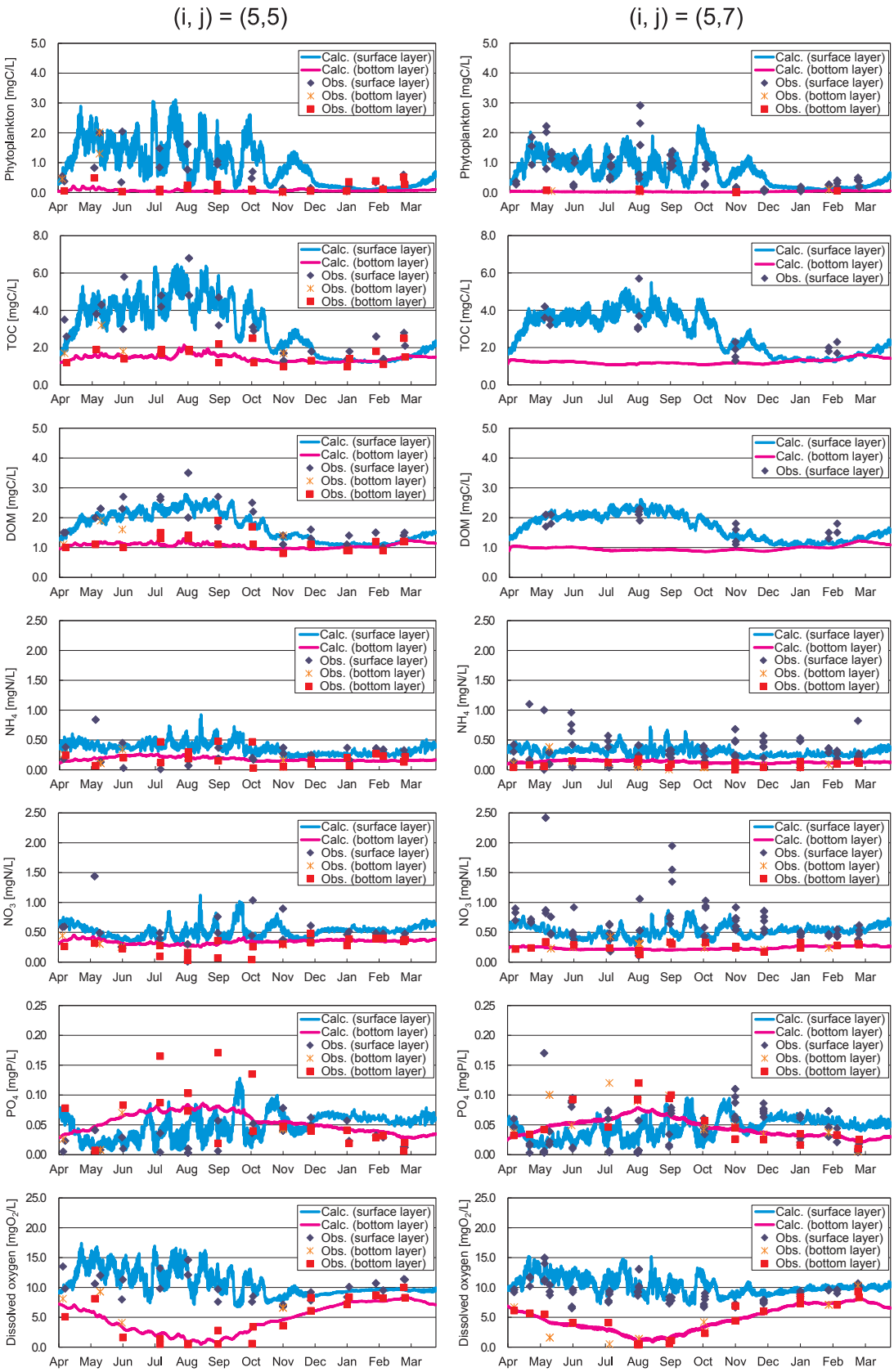

Fig. E1. Seasonal variations in the pelagic system, i.e., phytoplankton, TOC, DOC, NH_4-N, NO_3, PO_4-P, and dissolved oxygen at zones (i, j) = (5, 5) and (5, 7), comparison between the observed data (dots) and model outputs (lines).

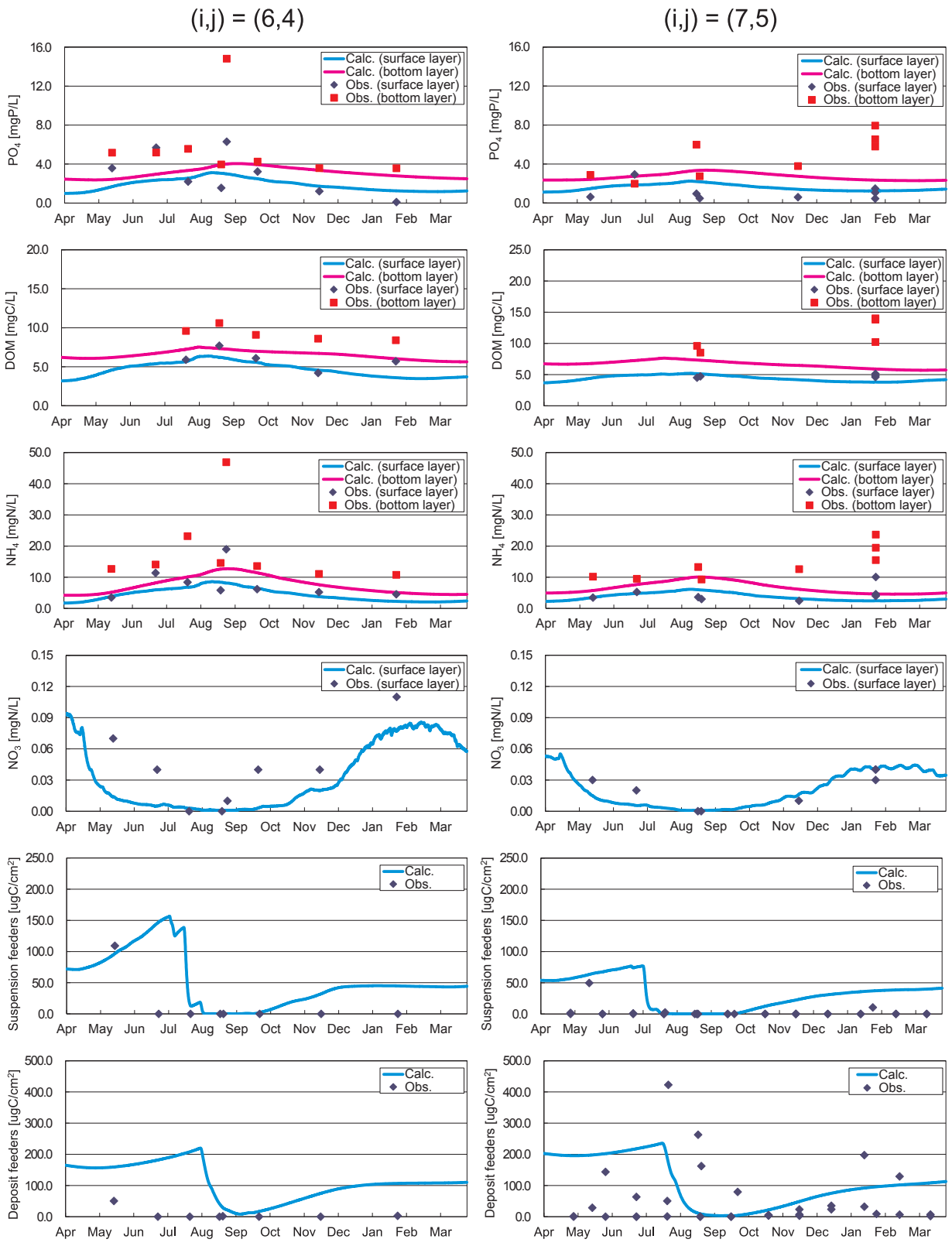

Fig. E2. Seasonal variations in the benthic system, i.e., PO_4-P, DOM, NH_4-N, NO_3-N, and dissolved oxygen at zones (i, j) = (6, 4) and (7, 5), comparisons between the observed data (dots) and model outputs (lines).

Appendix F. Summary of the hydrodynamic model

The hydrodynamic model simulates the three-dimensional physical field in the pelagic system of the estuary and demonstrates the long-term variability of the flow field, salt, and heat transport. The target area of the model is an estuary, i.e., a mesoscale (1 ~ 100 km), semi-closed coastal zone where the sea water is exchanged with the external ocean and is diluted by the inflow of freshwater from rivers. The model equations and algorithms of the hydrodynamic model are well described by (Nakata et al., 1983a,b). The model includes tidal forcing, surface winds, and local density gradients with realistic coastal topography and bathymetry described by computational grids/mesh. Under hydrostatic and *Boussinesq* approximations on a rotating Cartesian coordinate system, the model employs the equations of fluid motion, flow continuity, and conservation of heat and salt to determine the local distribution of model variables, i.e., mean velocity components, surface displacement, temperature, and salinity. The model equations of motion refer to a Cartesian coordinate system (Fig. F1) and are as follows:

(1) The equation of fluid motion in the x-direction

$$\frac{\partial u}{\partial t} = -u\frac{\partial u}{\partial x} - v\frac{\partial u}{\partial y} - w\frac{\partial u}{\partial z} + f_0 \cdot v - \frac{1}{\rho}\frac{\partial P}{\partial x} + \frac{\partial}{\partial x}\left(N_x\frac{\partial u}{\partial x}\right) + \frac{\partial}{\partial y}\left(N_y\frac{\partial u}{\partial y}\right) + \frac{\partial}{\partial z}\left(N_z\frac{\partial u}{\partial z}\right) \tag{F.1}$$

(2) The equation of fluid motion in the y-direction

$$\frac{\partial v}{\partial t} = -u\frac{\partial v}{\partial x} - v\frac{\partial v}{\partial y} - w\frac{\partial v}{\partial z} - f_0 \cdot u - \frac{1}{\rho}\frac{\partial P}{\partial y} + \frac{\partial}{\partial x}\left(N_x\frac{\partial v}{\partial x}\right) + \frac{\partial}{\partial y}\left(N_y\frac{\partial v}{\partial y}\right) + \frac{\partial}{\partial z}\left(N_z\frac{\partial v}{\partial z}\right) \tag{F.2}$$

(3) The equation of hydrostatic pressure approximation

$$-\frac{1}{\rho}\frac{\partial P}{\partial z} - g = 0 \tag{F.3}$$

(4) The equation of flow continuity

$$\frac{\partial u}{\partial x} + \frac{\partial v}{\partial y} + \frac{\partial w}{\partial z} = 0 \tag{F.4}$$

(5) The equation of conservation of heat

$$\frac{\partial T}{\partial t} = -u\frac{\partial T}{\partial x} - v\frac{\partial T}{\partial y} - w\frac{\partial T}{\partial z} + \frac{\partial}{\partial x}\left(K_x\frac{\partial T}{\partial x}\right) + \frac{\partial}{\partial y}\left(K_y\frac{\partial T}{\partial y}\right) + \frac{\partial}{\partial z}\left(K_z\frac{\partial T}{\partial z}\right) \tag{F.5}$$

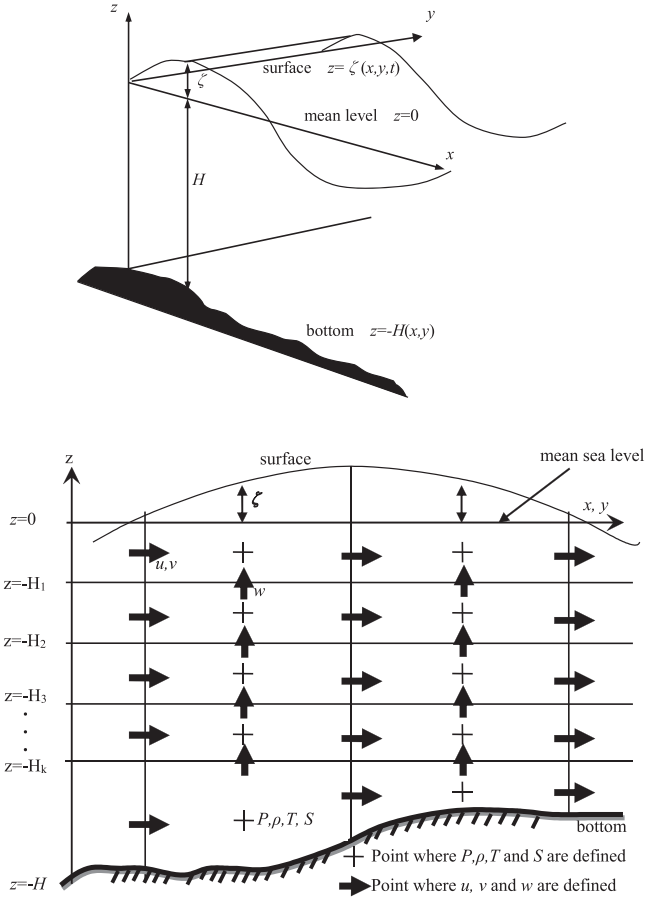

Fig. F1. Hydrodynamic model coordinates (upper) and multi-level layers in the vertical direction (lower).

(6) The equation of conservation of salt

$$\frac{\partial S}{\partial t} = -u\frac{\partial S}{\partial x} - v\frac{\partial S}{\partial y} - w\frac{\partial S}{\partial z} + \frac{\partial}{\partial x}\left(K_x\frac{\partial S}{\partial x}\right) + \frac{\partial}{\partial y}\left(K_y\frac{\partial S}{\partial y}\right) + \frac{\partial}{\partial z}\left(K_z\frac{\partial S}{\partial z}\right) \tag{F.6}$$

(7) The equation of state

$$\rho = \rho(S, T) \tag{F.7}$$

Where, t = time [s]; (x, y, z) = the Cartesian coordinate system with x and y measured in the horizontal plane of the undisturbed sea and z being the distance above that surface (henceforth, that surface is referred to as the mean sea level) [cm]; (u, v, w) = the velocities of the x, y, and z directions [cm·s^{-1}]; f_0 = Coriolis parameter [s^{-1}]; ρ = density of sea water [g·cm^{-3}]; P = pressure [g·cm^{-1}·s^{-2}]; g = acceleration of the earth's gravity [980·cm·s^{-2}]; H = the depth from the mean sea level to the bottom [cm]; T = the temperature of sea water [℃]; S = salinity[‰]; and (N_x, N_y, N_z) and (K_x, K_y, K_z) are eddy coefficients of viscosity and diffusion [cm^2·s^{-1}].

The assumptions implied in Eqs. (F.1) to (F.7) are as follow:

- (i) Eq. (F.4) assumes incompressible flow.
- (ii) Eq. (F.3) is the usual hydrostatic approximation involving the neglect of vertical acceleration.
- (iii) For the equation of state (F.7), Knudsen's expression is adopted. That is:

$$\rho = \frac{\sigma_t}{1000} + 1\ [g\cdot cm]^{-3}$$

$$\sigma_t = \sum_t + (\sigma_0 + 0.1324)\cdot\{1 - A_t + B_t(\sigma_0 - 0.1324)\}$$

$$\sigma_0 = -0.069 + 1.4708\cdot S - 0.00157S^2 + 0.0000398S^3$$

$$\sum_t = -\frac{(T-3.98)^2}{503.57}\cdot\frac{T + 283.0}{T + 67.26}$$

$$A_t = T(4.7867 - 0.098185T + 0.0010843T^2)\times 10^{-3}$$

$$B_t = T(18.03 - 0.8164T + 0.01667T^2)\times 10^{-6} \tag{F.8}$$

- (iv) The Coriolis parameter is constant (f-plane approximation).

From the vertical integration of Eq. (F.3), the following equation is obtained:

$$P = P_0 + g\int_z^\zeta \rho dz \tag{F.9}$$

Therefore, the terms of pressure gradient in Eqs. (F.1) and (F.2) are transformed as follows:

$$-\frac{1}{\rho}\frac{\partial P}{\partial x} = -g\frac{\partial \zeta}{\partial x} - \frac{g}{\rho}\int_z^\zeta \frac{\partial \rho}{\partial x}dz - \frac{1}{\rho}\frac{\partial P_0}{\partial x} \tag{F.10}$$

$$-\frac{1}{\rho}\frac{\partial P}{\partial y} = -g\frac{\partial \zeta}{\partial y} - \frac{g}{\rho}\int_z^\zeta \frac{\partial \rho}{\partial y}dz - \frac{1}{\rho}\frac{\partial P_0}{\partial y} \tag{F.11}$$

where P_0 = atmospheric pressure [g·cm^{-1}·s^{-2}] and ζ = tidal level from the mean sea level [cm].

From Eqs. (F.1),(F.4), and (F.10), Eq. (F.1) can be transformed into flux form as follow:

$$\frac{\partial u}{\partial t} = -\frac{\partial}{\partial x}(u^2) - \frac{\partial}{\partial y}(uv) - \frac{\partial}{\partial z}(uw) + f_0\cdot v - g\frac{\partial \zeta}{\partial x} - \frac{g}{\rho}\int_z^\zeta \frac{\partial \rho}{\partial x}dz - \frac{1}{\rho}\frac{\partial P_0}{\partial x} + \frac{\partial}{\partial x}\left(N_x\frac{\partial u}{\partial x}\right) + \frac{\partial}{\partial y}\left(N_y\frac{\partial u}{\partial y}\right) + \frac{\partial}{\partial z}\left(N_z\frac{\partial u}{\partial z}\right) \tag{F.12}$$

In the same way as the x-axis, for the y-axis, Eq. (F.2) is transformed as follows:

$$\frac{\partial v}{\partial t} = -\frac{\partial}{\partial x}(uv) - \frac{\partial}{\partial y}(v^2) - \frac{\partial}{\partial z}(vw) - f_0\cdot u - g\frac{\partial \zeta}{\partial y} - \frac{g}{\rho}\int_z^\zeta \frac{\partial \rho}{\partial y}dz - \frac{1}{\rho}\frac{\partial P_0}{\partial y} + \frac{\partial}{\partial x}\left(N_x\frac{\partial v}{\partial x}\right) + \frac{\partial}{\partial y}\left(N_y\frac{\partial v}{\partial y}\right) + \frac{\partial}{\partial z}\left(N_z\frac{\partial v}{\partial z}\right) \tag{F.13}$$

In addition, from Eqs. (F.4),(F.5), and (F.6), the equations of conservation of heat and salt are transformed as follows:

$$\frac{\partial T}{\partial t} = -\frac{\partial}{\partial x}(uT) - \frac{\partial}{\partial y}(vT) - \frac{\partial}{\partial y}(wT) + \frac{\partial}{\partial x}\left(K_x\frac{\partial T}{\partial x}\right) + \frac{\partial}{\partial y}\left(K_y\frac{\partial T}{\partial y}\right) + \frac{\partial}{\partial z}\left(K_z\frac{\partial T}{\partial z}\right) \tag{F.14}$$

$$\frac{\partial S}{\partial t} = -\frac{\partial}{\partial x}(uS) - \frac{\partial}{\partial y}(vS) - \frac{\partial}{\partial y}(wS) + \frac{\partial}{\partial x}\left(K_x\frac{\partial S}{\partial x}\right) + \frac{\partial}{\partial y}\left(K_y\frac{\partial S}{\partial y}\right) + \frac{\partial}{\partial z}\left(K_z\frac{\partial S}{\partial z}\right) \tag{F.15}$$

Also, the dynamic boundary condition $D\zeta/Dt = 0$ at surface (z = ζ), which means that water does not pass through the sea surface, and the dynamic boundary condition $DH_b/Dt = 0$ at sea bottom (z = -H_b), which means that no water passes through the sea bottom are satisfied. By using these boundary conditions, the following equation describing the dynamics of the surface level can be obtained:

$$\frac{\partial \zeta}{\partial t} = -\frac{\partial}{\partial x}\left(\int_{-H}^{\zeta} u dz\right) - \frac{\partial}{\partial y}\left(\int_{-H}^{\zeta} v dz\right) \tag{F.16}$$

These seven Eqs. (F.4),(F.8), (F.12), (F.13), (F.14), (F.15), and (F.16) are the model equations of the hydrodynamic model. The model is

calculated by the finite volume method (FVM) and by the explicit leap frog computational scheme, whose algorithm conserves the mass of model compartments (temperature and salinity) and the volume of sea water.

The vertical mixing process is parameterized with a turbulence model with a second-moment closure, which determines local distributions of the turbulent kinetic energy, k [$cm^2 \cdot s^{-2}$], and the mixing length, l [cm], by means of well-established k-kl equations (e.g., Blumberg and Mellor, 1978; Mellor and Yamada, 1982).

As for the boundary conditions, the conditions at (1) land boundaries (coastal line), (2) open-sea boundaries (bay mouse), (3) the air-water interface (sea surface), and (4) the sediment-water interface (sea bottom) are set on the hydrodynamic model. At (1) land boundaries (coastal line), the free-slip condition is applied to the momentum (current):

$$\mathbf{u} \cdot \mathbf{n} = 0, \ \frac{\partial \mathbf{u}_t}{\partial n} = 0 \tag{F.17}$$

For the temperature and salinity at (1) land boundaries, the following condition (i.e., temperature and salinity are not transported at land boundaries) is applied:

$$\frac{\partial T}{\partial n} = \frac{\partial S}{\partial n} = 0 \tag{F.18}$$

where $\mathbf{u}$ is the current vector [$cm \cdot s^{-1}$] and $\mathbf{n}$ [-] is the normal vector to the coastline (outward directed from ocean area). n denotes the element of normal direction of the coastal line. t denotes the element of tangential direction of the coastal line.

At (2) open-sea boundaries (bay mouse), the sea-surface elevation, ζ, described by trigonometric function is given and a free-stream condition is applied to the momentum (current). For the temperature and concentration of salinity, the values of their inflow from the outside to the inside of the calculation area are specified by prescribed functions, and the values for the outflow from the inside to the outside set the free-stream condition:

$$\zeta = \zeta_0 + \sum_i A_i cos(\omega_i t - \delta) \tag{F.19}$$

$$\frac{\partial \mathbf{u}_t}{\partial n} = 0 \tag{F.20}$$

$$\frac{\partial T}{\partial n} = \frac{\partial S}{\partial n} = 0 \text{ (for outflow side)} \tag{F.21}$$

$$T = T_0, \ S = S_0 \text{ (for inflow side)} \tag{F.22}$$

Where, A_i [cm] is the amplitude of each tidal element, ω_i is the frequency of each tidal element, δ [$radian \cdot s^{-1}$] is the angle of delay, and T_0 [℃] and S_0 [‰] are the prescribed values of temperature and salinity, respectively, at the open-sea boundary.

As for the boundary conditions at the (3) air-water interface ($z = \zeta$), the stress caused by the wind, heat flux, and the free surface condition are given as follows:

$$\rho N_z \frac{\partial u}{\partial z} = \tau_x^s \tag{F.23}$$

$$\rho N_z \frac{\partial v}{\partial z} = \tau_y^s \tag{F.24}$$

$$K_z \frac{\partial T}{\partial z} = Q \tag{F.25}$$

$$\frac{D\zeta}{Dt} = 0 \tag{F.26}$$

where τ_x^s and τ_y^s [$g \cdot cm^{-1} \cdot s^{-2}$] are the wind stresses and Q [$℃ \cdot cm \cdot s^{-1}$]is the downward heat flux.

The final boundary condition at the (4) sea bottom ($z = -H_b$) is the slip condition for the bottom stress and the dynamic boundary condition as follows:

$$\rho N_z \frac{\partial u}{\partial z} = \tau_x^b \tag{F.27}$$

$$\rho N_z \frac{\partial v}{\partial z} = \tau_y^b \tag{F.28}$$

$$K_z \frac{\partial T}{\partial z} = 0 \tag{F.29}$$

$$\frac{DH_b}{Dt} = 0 \tag{F.30}$$

Where, τ_x^b, τ_y^b [$g \cdot cm^{-1} \cdot s^{-2}$] are friction stresses at the sediment-water interface (sea bottom).

References

Admiraal, W., Peletier, H., Zomer, H., 1982. Observations and experiments on the population dynamics of epipelic diatoms from an estuarine mudflat. Estuar. Coast. Mar. Sci. 14, 471–487.

Algesten, G., Brydsten, L., Jonsson, P., Kortelainen, P., Lofgren, S., Rahm, L., Raike, A., Sobek, S., Tranvik, L., Wikner, J., Jansson, M., 2006. Organic carbon budget for the Gulf of Bothnia. J. Mar. Syst. 63, 155–161.

Alongi, D.M., Murdiyarso, D., Fourqurean, J.W., Kauffman, J.B., Hutahaean, A., Crooks, S., Lovelock, C.E., Howard, J., Herr, D., Fortes, M., Pidgeon, E., Wagey, T., 2016. Indonesia's blue carbon: a globally significant and vulnerable sink for seagrass and

mangrove carbon. Wetl. Ecol. Manag. 24, 3–13.
Archer, D., Brovkin, V., 2008. The millennial atmospheric lifetime of anthropogenic CO2. Clim. Change 90, 283–297.
Artioli, Y., Blackford, J.C., Butenschon, M., Holt, J.T., Wakelin, S.L., Thomas, H., Borges, A.V., Allen, J.I., 2012. The carbonate system in the North Sea: sensitivity and model validation. J. Mar. Syst. 102, 1–13.
Aumont, O., Maier-Reimer, E., Blain, S., Monfray, P., 2003. An ecosystem model of the global ocean including Fe, Si, P colimitations. Glob. Biogeochem. Cycles 17, 1060.
Baretta, J.W., Ruardij, P., 1988. Tidal flat estuaries, simulation and analysis of the Ems estuary. Ecological Studies, vol. 71 Springer-Verlag.
Berner, R.A., 1980. Early Diagenesis: a Theoretical Approach. Princeton University Press, Princeton, New Jersey 241 pp.
Blumberg, A.F., Mellor, G.L., 1978. A coastal ocean numerical model. In: Sundermann, J., Holz, K.P. (Eds.), Mathematical Modeling of Estuarine Physics, Proceedings of an International Symposium. Hamburg, August 24 to 26, 1978, Springer-Verlag, Berlin. pp. 203–219.
Borges, A.V., Abril, G., 2011. Carbon dioxide and methane dynamics in estuaries. Treaties on Estuarine and Coastal Science 5. Elsevier, pp. 199.
Broecker, W.S., Takahashi, T., 1978. The relationship between lysocline depth and in situ carbonate ion concentration. Deep Sea Res. 25, 65–95.
Butenschoen, M., Clark, J., Aldridge, J.N., Allen, J.I., Artioli, Y., Blackford, J., Bruggeman, J., Cazenave, P., Ciavatta, S., Kay, S., Lessin, G., van Leeuwen, S., van der Molen, J., de Mora, L., Polimene, L., Sailley, S., Stephens, N., Torres, R., 2016. ERSEM 15.06: a generic model for marine biogeochemistry and the ecosystem dynamics of the lower trophic levels. Geosci. Model. Dev. 9, 1293–1339.
Cai, W.J., 2011. Estuarine and coastal ocean carbon paradox: CO2 sinks or sites of terrestrial carbon incineration? Annu. Rev. Mar. Sci. 3, 123–145.
Cammen, L.M., 1980. Ingestion rate: an empirical model for aquatic deposit feeders and detritivores. Oecologia 44, 303–310.
Cerco, C.F., Noel, M.R., Kim, S.C., 2006. Three-dimensional management model for Lake Washington, part II: eutrophication modeling and skill assessment. Lake Reserv. Manag. 22, 115–131.
Chen, C.T.A., Huang, T.H., Chen, Y.C., Bai, Y., He, X., Kang, Y., 2013. Air-sea exchanges of CO2 in the world's coastal seas. Biogeosciences 10, 6509–6544.
Chen, C.T.A., Huang, T.H., Fu, Y.H., Bai, Y., He, X.Q., 2012. Strong sources of CO2 in upper estuaries become sinks of CO2 in large river plumes. Curr. Opin. Environ. Sustain. 4, 179–185.
Chmura, G.L., Anisfeld, S.C., Cahoon, D.R., Lynch, J.C., 2003. Global carbon sequestration in tidal, saline wetland soils. Glob. Biogeochem. Cycles 17, 1111.
Conover, R.J., 1978. Transformation of organic matter. In: Kinne, O. (Ed.), Marine Ecology, vol. IV. Dynamics. Wiley, New York, pp. 221–499.
Dickson, A.G., 1981. An exact definition of total alkalinity and a procedure for the estimation of alkalinity and inorganic carbon from titration data. Deep Sea Res. 28, 609–623.
Dickson, A.G., 1990. Thermodynamics of the dissociation of boric-acid in potassium-chloride solutions from 273.15-K TO 318.15-K. J. Chem. Eng. Data 35, 253–257.
Dickson, A.G., Goyet, C. (Eds.), 1994. Handbook of Methods for the Analysis of the Various Parameters of Carbon Dioxide System in Sea Water, Version 2, DOE CO2 Science Term Report. US Department of Energy, Washington, DC.
Dickson, A.G., Sabine, C.L., Christian, J.R., 2007. Guide to Best Practices for Ocean CO2 Measurements PICES Special Publication 3, IOCCP Report no. 8. 191pp.. .
Donato, D.C., Kauffman, J.B., Murdiyarso, D., Kurnianto, S., Stidham, M., Kanninen, M., 2011. Mangroves among the most carbon-rich forests in the tropics. Nat. Geosci. 4, 293–297.
Duarte, C.M., Losada, I.J., Hendriks, I.E., Mazarrasa, I., Marbà, N., 2013. The role of coastal plant communities for climate change mitigation and adaptation. Nat. Clim. Change 3, 961–968. http://dx.doi.org/10.1038/nclimate1970.
Duarte, C.M., 2017. Reviews and syntheses: hidden forests, the role of vegetated coastal habitats in the ocean carbon budget. Biogeosciences 14, 301–310.
Duarte, C.M., Cebrian, J., 1996. The fate of marine autotrophic production. Limnol. Oceanogr. 41, 1758–1766.
Duarte, C.M., Middelburg, J.J., Caraco, N., 2005. Major role of marine vegetation on the oceanic carbon cycle. Biogeosciences 2, 1–8.
Emerson, S., Hedges, J.L., 1988. Processes controlling the organic carbon content of open ocean sediments. Paleoceanography 3, 621–634.
Epply, R.W., Rogers, J.N., McCarthy, J.J., 1969. Half saturation constants for uptake of nitrate and ammonium by marine phytoplankton. Limnol. Oceanogr. 14, 912–920.
Eyre, B.D., McKee, L.J., 2002. Carbon, nitrogen, and phosphorus budgets for a shallow subtropical coastal embayment (Moreton Bay, Australia). Limnol. Oceanogr. 47, 1043–1055.
Falkowski, P., Scholes, R.J., Boyle, E., Canadell, J., Canfield, D., Elser, J., Gruber, N., Hibbard, K., Hogberg, P., Linder, S., Mackenzie, F.T., Moore, B., Pedersen, T., Rosenthal, Y., Seitzinger, S., Smetacek, V., Steffen, W., 2000. The global carbon cycle: a test of our knowledge of earth as a system. Science 290, 291–296.
Fasham, M.J.R., Ducklow, H.W., McKelvie, S.M., 1990. A nitrogen-based model of plankton dynamics in the oceanic mixed layer. J. Mar. Res. 48, 591–639.
Fennel, K., Hetland, R., Feng, Y., DiMarco, S., 2011. A coupled physical-biological model of the Northern Gulf of Mexico shelf: model description, validation and analysis of phytoplankton variability. Biogeosciences 8, 1881–1899.
Flynn, K.J., 2010. Ecological modelling in a sea of variable stoichiometry: dysfunctionality and the legacy of redfield and monod. Prog. Oceanogr. 84, 52–65.
Fourqurean, J.W., Duarte, C.M., Kennedy, H., Marba, N., Holmer, M., Mateo, M.A., Apostolaki, E.T., Kendrick, G.A., Krause-Jensen, D., McGlathery, K.J., Serrano, O., 2012. Seagrass ecosystems as a globally significant carbon stock. Nat. Geosci. 5, 505–509.
Frankignoulle, M., Abril, G., Borges, A., Bourge, I., Canon, C., DeLille, B., Libert, E., Theate, J.M., 1998. Carbon dioxide emission from European estuaries. Science 282, 434–436.
Fuhs, W.G., Demmerle, S.D., Canelli, E., and Chen, M., 1972. Characterization of phosphorus-limited plankton algae (with reflections on the limiting nutrient concept). In: Likens, G.E., (Ed.), Nutrients and Eutrophication. Spec. Symp. Vol. 1, Am. Soc. Limnology and Oceanography. Allen Press, Lawrence, KS, pp. 113–133.
Geider, R.J., MacIntyre, H.L., Kana, T.M., 1997. Dynamic model of phytoplankton growth and acclimation: responses of the balanced growth rate and the chlorophyll a:carbon ratio to light, nutrient-limitation and temperature. Mar. Ecol. Prog. Ser. 148, 187–200.
Hiroshima Environment & Health Association, 2002. Report about Ecological Improvement of Sediment Quality Using Benthic Algae in Seto Inland Sea. (in Japanese) web site http://nippon.zaidan.info/seikabutsu/2001/00614/mokuji.htm.
Hiwatari, T., Kohata, K., Iijima, A., 2002. Nitrogen budget of the bivalve mactra veneriformis, and its significance in benthic-pelagic systems in the sanbanse area of Tokyo Bay. Estuar. Coast. Self Sci. 55, 299–308.
Hoffert, M.I., Wey, Y.C., Callegari, A.J., Broecker, W.S., 1979. Atmospheric response to deep-sea injections of fossil-fuel carbon-dioxide. Clim. Change 2, 53–68.
Horiguchi, F., 2001. Numerical simulations of seasonal cycle of Tokyo Bay using an ecosystem model. J. Adv. Mar. Sci. Technol. Soc. 7 (1&2), 1–30 (in Japanese with English abstract).
Houghton, J.T., Intergovernmental Panel on Climate Change. Working Group I., 2001. Climate change 2001: the scientific basis: Contribution of Working Group I to the Third Assessment Report of the Intergovernmental Panel on Climate Change. Cambridge University Press, Cambridge, UK; pp. 881.
Ishikawa, M., Nishimura, H., 1983. A new method of evaluating the mineralization of particulate and dissolved photoassimilated organic matter. J. Oceanogr. Soc. Jpn. 39 (2), 29–42.
Isono, R., Kita, J., Kishida, C., 1998. Upper temperature effect on rates of growth and oxygen consumption of the Japanese little neck clam, Ruditapes philippinarum. Nippon Suisan Gakkaishi 64 (3), 373–376 (in Japanese with English abstract).
Japan Environmental Management Association for Industry, 1998. Survey Report of the Water Quality Pollution Mechanism in Mikawa Bay (in Japanese). .
Jørgensen, S.E. (Ed.), 1979. Handbook of Environmental Data and Ecological Parameters. International Society for Ecological Modelling Pergamon Press, Amsterdam, pp. 1162.
Jørgensen, S.E., Nielsen, S.N., Jørgensen, L.A., 1991. Handbook of Ecological Parameters and Ecotoxicology. Elsevier Science Publishers, Amsterdam, pp. 1263.
Jørgensen, S.E., Bendoricchio, G., 2001. third ed. Fundamentals of Ecological Modelling: Developments in Environmental Modelling, vol. 21 Elsevier, New York 530 pp.
Kakino, J., 1982. Effects of Ao-Shio on the Mortality in Manila. Clams. Bulletin of Chiba Prefectural Fisheries Research Institute 40. pp. 1–6 (in Japanese).
Kamio, K., Nomura, M., Nakamura, Y., Kuwae, T., Inoue, T., Konuma, S., 2004. Oxygen variation of the tidal flat overlying water. Proceedings of the 2004 Spring Annual Meeting of The Oceanographic Society of Japan. pp. 199 (in Japanese).
Kone, Y.J.M., Abril, G., Kouadio, K.N., Delille, B., Borges, A.V., 2009. Seasonal variability of carbon dioxide in the rivers and lagoons of Ivory Coast (West Africa). Estuar. Coasts 32, 246–260.
Kremer, J.N., Nixon, S.W., 1978. A Coastal Marine Ecosystem, Simulation and Analysis. Springer-Verlag, Berlin, pp. 217.
Kubo, A., Kanda, J., 2017. Seasonal variations and sources of sedimentary organic carbon in Tokyo Bay. Mar. Pollut. Bull. 114, 637–643.
Kubo, A., Maeda, Y., Kanda, J., 2017. A significant net sink for CO2 in Tokyo Bay. Sci. Rep. 7.
Kubo, A., Yamamoto-Kawai, M., Kanda, J., 2015. Seasonal variations in concentration and lability of dissolved organic carbon in Tokyo Bay. Biogeosciences 12, 269–279.
Kurashige, H., 1942. Resistance of Paphia philippinarum adams et reeve to lack of oxygen. J. Oceanogr. Soc. Jpn. 1 (1–2), 123–132 (in Japanese).
Kuwae, T., 2001. Biogeochemical Roles of Benthic Microorganisms in Intertidal Sandflats. Ph. D. Thesis. Kyoto University 93 pp.
Kuwae, T., Inoue, T., Miyoshi, E., Konuma, S., Hosokawa, S., Nakamura, Y., 2005. Modeling the coastal marine ecosystem coupled with tidal flats based on the study of oxygen cycling in sediments. Report of Program for Promoting Fundamental Transport Technology Research. Japan Railway Construction, Transport and Technology Agency, pp. 262–423 (in Japanese).
Kuwae, T., Kanda, J., Kubo, A., Nakajima, F., Ogawa, H., Sohma, A., Suzumura, M., 2016. Blue carbon in human-dominated estuarine and shallow coastal systems. Ambio 45, 290–301.
Lancelot, C., Spitz, Y., Gypens, N., Ruddick, K., Becquevort, S., Rousseau, V., Lacroix, G., Billen, G., 2005. Modelling diatom and phaeocystis blooms and nutrient cycles in the Southern Bight of the North Sea: the MIRO model. Mar. Ecol. Prog. Ser. 289, 63–78.
Laruelle, G.G., Durr, H.H., Lauerwald, R., Hartmann, J., Slomp, C.P., Goossens, N., Regnier, P.A.G., 2013. Global multi-scale segmentation of continental and coastal waters from the watersheds to the continental margins. Hydrol. Earth Syst. Sci. 17, 2029–2051.
Macedo, M.F., Duarte, P., Mendes, P., Ferreira, J.G., 2001. Annual variation of environmental variables, phytoplankton species composition and phytosynthetic parameters in a coastal lagoon. J. Plankton Res. 23 (7), 719–732.
Mahmud, M.A., Elumalai, N.K., Upama, M.B., Wang, D., Puthen-Veettil, B., Haque, F., Wright, M., Xu, C., Pivrikas, A., Uddin, A., 2017. Controlled ostwald ripening mediated grain growth for smooth perovskite morphology and enhanced device performance. Sol. Energy Mater. Sol. Cells 167, 87–101.
Marshall, S.M., Orr, A.P., 1955a. Experimental feeding of the copepod Calanus finmarchicus on phytoplankton cultures labeled with radioactive carbon. Pap. Mar. Biol. Oceanogr. Deep-Sea Res. 3 (Suppl), 110–114.
Marshall, S.M., Orr, A.P., 1955b. On the biology of Calanus finmarchicus. VIII. Food

uptake, assimilation and excretion in adult and stage V. Calanus. J. Mar. Biol. Assoc. U. K. 34, 495–529.
Matsunaga, K., 1981. Studies on the decomposition processes of phytoplanktonic organic matter. Japn. J. Limnol. 42 (4), 220–229.
McLeod, E., Chmura, G.L., Bouillon, S., Salm, R., Bjork, M., Duarte, C.M., Lovelock, C.E., Schlesinger, W.H., Silliman, B.R., 2011. A blueprint for blue carbon: toward an improved understanding of the role of vegetated coastal habitats in sequestering CO2. Front. Ecol. Environ. 9, 552–560.
Mehrbach, C., Culberson, C.H., Hawley, J.E., Pytkowicz, R.M., 1973. Measurement of apparent dissociation-constants of carbonic-acid in seawater at atmospheric-pressure. Limnol. Oceanogr. 18, 897–907.
Meire, L., Soetaert, K.E.R., Meysman, F.J.R., 2013. Impact of global change on coastal oxygen dynamics and risk of hypoxia. Biogeosciences 10, 2633–2653.
Mellor, G.L., Yamada, T., 1982. Development of a turbulent closure model for geophysical fluid problems. Rev. Geophys. 20, 851–875.
Millero, F.J., 1995. Thermodynamics of the carbon-dioxide system in the oceans. Geochim. Et Cosmochim. Acta 59, 661–677.
Murdiyarso, D., Purbopuspito, J., Kauffman, J.B., Warren, M.W., Sasmito, S.D., Donato, D.C., Manuri, S., Krisnawati, H., Taberima, S., Kurnianto, S., 2015. The potential of Indonesian mangrove forests for global climate change mitigation. Nat. Clim. Change 5, 1089–1092.
Nakata, K., Horiguchi, F., Taguchi, K., Setoguchi, Y., 1983a. Three dimensional simulation of tidal current in oppa estuary. Bull. Natl. Res. Inst. For. Pollut. Resour. 12 (3), 17–36 (in Japanese).
Nakata, K., Horiguchi, F., Taguchi, K., Setoguchi, Y., 1983b. Three dimensional eco-hydrodynamical model in coastal region. Bull. Natl. Res. Inst. For. Pollut. Resour. 13 (2), 119–134 (in Japanese).
National Institute for Land and Infrastructure Management, 2006. Integrated Environmental Monitoring at Tokyo Bay (2002–2003) (in Japanese) web site. http://www.nilim.go.jp/.
Nishikawa, T., Miyahara, K., Nagai, S., 2002. The growth response of Coscinodiscus wailesii Gran (Bacillariophyceae) as a function of irradiance isolated from Harima-Nada, Seto Inland Sea. Japan Bull. Plankton Soc. 49 (1), 1–8 (in Japanese with English abstract).
Ogawa, N., Ogura, N., 1997. Dynamics of particulate organic matter in the tamagawa estuary and inner Tokyo Bay. Estuar. Coast. Shelf Sci. 44, 263–273.
Ogura, N., 1972. Decomposition of dissolved organic matter derived from dead phytoplankton. In: Takenouti, A.Y. (Ed.), Biological Oceanography of the Northern Pacific Ocean. Idemitsu Shoten, Tokyo, pp. 507–515.
Ogura, N., 1975. Further studies on decomposition of dissolved organic matter in coastal seawater. Mar. Biol. 31, 101–111.
Oguz, T., 2002. The role of physical processes controlling the oxycline and suboxic layer structures in the Black Sea. Glob. Biogeochem. Cycles 16 (2), 101029–101042.
Pritchard, D.W., 1967. What is an estuary: physical viewpoint. In: Lauff, G.H. (Ed.), Estuaries. AAAS Publication no. 83, Washington, DC, pp. 3–5.
Reed, D.C., Slomp, C.P., Gustafsson, B.G., 2011. Sedimentary phosphorus dynamics and the evolution of bottom-water hypoxia: a coupled benthic-pelagic model of a coastal system. Limnol. Oceanogr. 56, 1075–1092.
Rosenfeld, J.K., 1979. Ammonium adsorption in nearshore anoxic sediments. Limnol. Oceanogr. 24, 356–364.
Sato, T., Miyajima, T., Ogawa, H., Umezawa, Y., Koike, I., 2006. Temporal variability of stable carbon and nitrogen isotopic composition of size-fractionated particulate organic matter in the hypertrophic Sumida River estuary of Tokyo Bay. Jpn. Estuar. Coast. Shelf Sci. 68, 245–258.
Soetaert, K., Herman, P.M.J., Middleburg, J.J., 1996. A model of early diagenetic processes from the shelf to abyssal depth. Geochimica et Cosmochimica Acta 60 (6), 1019–1040.
Soetaert, K., Herman, P.M.J., Middelburg, J.J., Heip, C., Smith, C.L., Tett, P., Wild-Allen, K., 2001. Numerical modelling of the shelf break ecosystem: reproducing benthic and pelagic measurements. Deep-Sea Res. 48 (Pt. II), 3141–3177.
Soetaert, K., Hofmann, A.F., Middelburg, J.J., Meysman, F.J.R., Greenwood, J., 2007. The effect of biogeochemical processes on pH. Mar. Chem. 105 (1–2), 30–51.
Soetaert, K., Middelburg, J.J., 2009. Modeling eutrophication and oligotrophication of shallow-water marine systems: the importance of sediments under stratified and well-mixed conditions. Hydrobiologia 629, 239–254.
Sohma, A., Kakio, T., Sekiguchi, Y., Akai, M., 2005. Introduction of the global ocean ecosystem model "DONGRI" and its implementation to investigate the biochemical effects on global warming. Proceedings of the 7th International Conference on Greenhouse Gas Control Technologies, vol. 2, 2389–2393.
Sohma, A., Sekiguchi, Y., Kuwae, T., Nakamura, Y., 2008. A benthic-pelagic coupled ecosystem model to estimate the hypoxic estuary including tidal flat – model description and validation of seasonal/daily dynamics. Ecol. Model. 215, 10–39.
Solomon, S., 2007. Intergovernmental panel on climate change., Intergovernmental panel on climate change. Working group I. Climate Change 2007: the Physical Science Basis: Contribution of Working Group I to the Fourth Assessment Report of the Intergovernmental Panel on Climate Change. Cambridge University Press, Cambridge; New York viii, 996 pp.
Sorai, M., Ohsumi, T., 2005. Ocean uptake potential for carbon dioxide sequestration. Geochem. J. 39, 29–45.
Stock, C.A., Dunne, J.P., John, J.G., 2014. Global-scale carbon and energy flows through the marine planktonic food web: an analysis with a coupled physical-biological model. Prog. Oceanogr. 120, 1–28.
Strickland, J.D.H., 1965. Chemical composition of phytoplankton and method for measuring plant bio-mass, practical considerations composition ratios. Chem. Oceanogr. 1, 514–518.
Suschenya, L.M., 1970. Food rations, metabolism, and growth of crustaceans. In: Steele, J.H. (Ed.), Marine Food Chains. University of California Press, Berkeley, CA.
Valiela, I., 1984. Marine Ecological Processes. Springer, New York, pp. 1–546.
Wanninkhof, R., McGillis, W.R., 1999. A cubic relationship between air-sea CO2 exchange and wind speed. Geophys. Res. Lett. 26, 1889–1892.
Weiss, R.F., 1974. Carbon dioxide in water and seawater: the solubility of non-ideal gas. Mar. Chem. 2, 203–215.
Wild-Allen, K., Herzfeld, M., Thompson, P.A., Rosebrock, U., Parslow, J., Volkman, J.K., 2010. Applied coastal biogeochemical modelling to quantify the environmental impact of fish farm nutrients and inform managers. J. Mar. Syst. 81, 134–147.
Wolf-Gladrow, D.A., Zeebe, R.E., Klaas, C., Kortzinger, A., Dickson, A.G., 2007. Total alkalinity: the explicit conservative expression and its application to biogeochemical processes. Mar. Chem. 106, 287–300.
Yakushev, E.V., Protsenko, E.A., Bruggeman, J., Wallhead, P., Pakhomova, S.V., Yakubov, S.K., Bellerby, R.G.J., Couture, R.M., 2017. Bottom RedOx model (BROM v.1.1): a coupled benthic-pelagic model for simulation of water and sediment biogeochemistry. Geosci. Model. Dev. 10, 453–482.
Yamamuro, M., Koike, I., 1993. Nitrogen metabolism of the filter feeding bivalve Corbicula Japonica and its significance in primary production of a brackish lake in Japan. Limnol. Oceanogr. 38, 997–1007.
Yanagi, T., Saino, T., Ishimaru, T., Uye, S., 1993. A carbon budget in Tokyo Bay. J. Oceanogr. 49, 249–256.
Yool, A., Popova, E.E., Anderson, T.R., 2013. MEDUSA-2.0: an intermediate complexity biogeochemical model of the marine carbon cycle for climate change and ocean acidification studies. Geosci. Model. Dev. 6, 1767–1811.
Zavatarelli, M., Pinardi, N., 2003. The adriatic Sea modelling system: a nested approach. Ann. Geophys. 21, 345–364.
Zillioux, E., 1970. Ingestion and assimilation in laboratory cultures of acartia. Technical Report. the National Marine Water Quality Laboratory, EPA, Narragansett, RI.